THESIS REPORT

Master's Degree

Development of a Prototype System for On-Line Monitoring of Surface Roughness Using Fractal Geometry

by S. Gopalakrishnan
Advisor: G. Zhang

M.S. 94-9

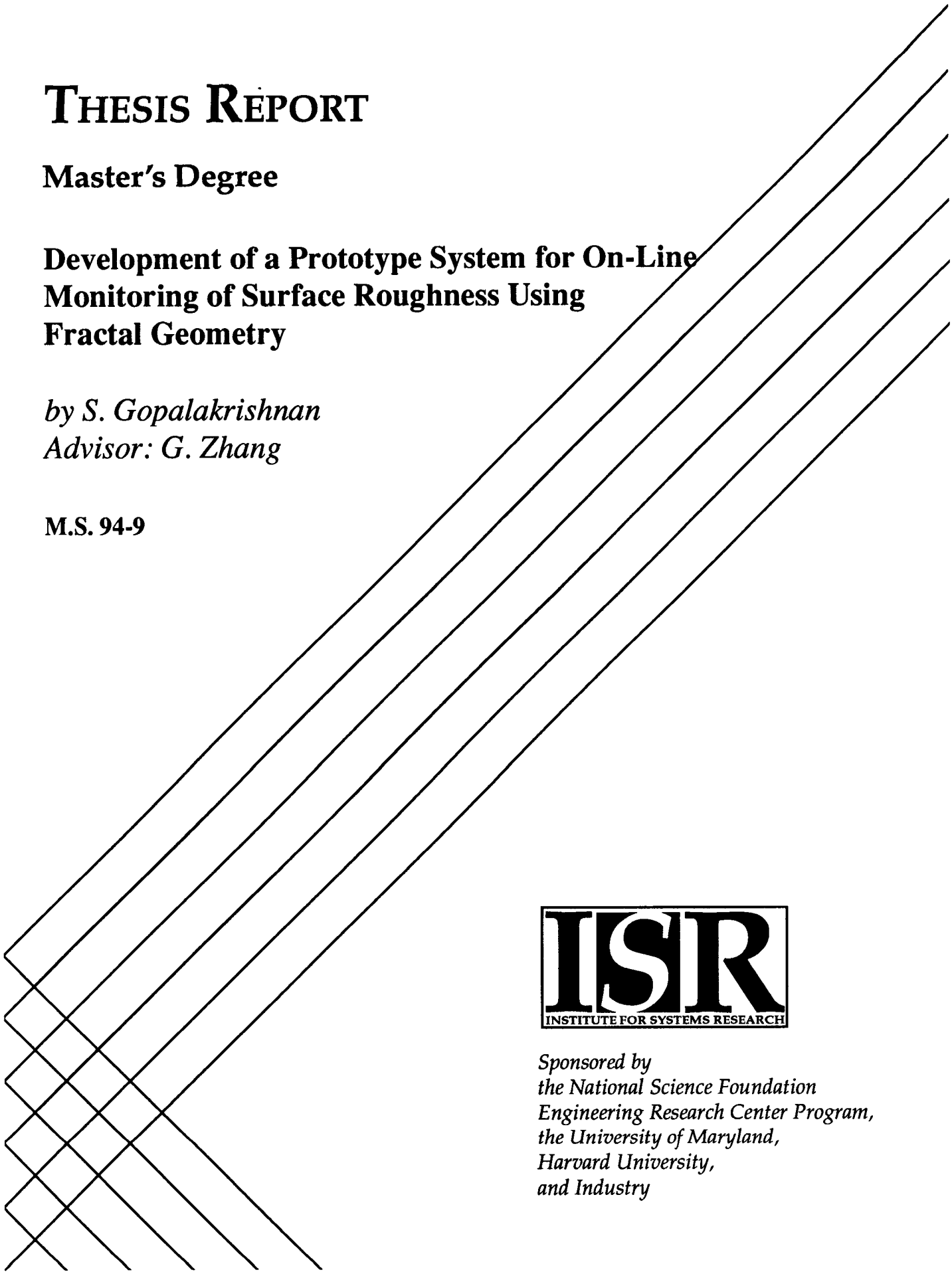

Sponsored by
the National Science Foundation
Engineering Research Center Program,
the University of Maryland,
Harvard University,
and Industry

Abstract

Title of Thesis: Development of a Prototype System for On-Line Monitoring of Surface Roughness using Fractal Geometry

Name of degree canditate: Shivakumar Gopalakrishnan

Degree and year: Master of Science, 1994

Thesis directed by: Dr. Guangming Zhang
Department of Mechanical Engineering and
Institute of Systems Research

On-line measurement of surface roughness is an important element in a Computer Integrated Manufacturing (CIM) environment. Current methods of contact measurement are not suitable as they interfere with the machining process. Optical methods, such as laser profilometry, in general, use expensive and large equipment, which pose difficulties in the implementation on the machine tool for on-line monitoring. This thesis presents an optical area based surface characterization technique, which applies fractal geometry and basic light scattering principles, to correlate surface roughness and fractal dimension. The unique contribution of this work is that the theory of electromagnetic scattering observed in rough surfaces and the fractal nature of the machined surfaces, are used to implement an in-process surface quality measurement. Fractal geometry is used to describe the surface

topography of the machined surface. Fractal dimension is found to be a parameter that can be used to estimate the surface roughness of machined surfaces.

The surface roughness of the machined surface is estimated by analyzing the image obtained from a CCD camera. An algorithm, which calculates the fractal dimension of the image, is incorporated within the image processing software to accomplish on-line monitoring of surface roughness. A calibration curve is generated by measuring the fractal dimension of samples of known surface roughness. This curve is then used for on-line monitoring of surface roughness. The capabilities and future potential of this system are demonstrated.

Dedication

To my Parents

Acknowledgments

I thank Dr. Guangming Zhang for his continuous support throughout this project. Without his guidance, this work would not have been accomplished. I would also like to thank Mr. Don Devoe for his valuable suggestions during the initial stages of this work. I thank Mr. Song of National Institute of Standards and Technology for his guidance in the use of metrology instruments.

Table of Contents

List of Tables

List of Figures

Nomenclature

A	Set of points contained in the curve
α	constant
a	scaling constant in W-M function
$C(\lambda)$	Ratio of spectral power due to wavelength (λ) to the total incident power
D	Fractal dimension
E	number of arguments in fBm
ε	Variable denoting the size of the segment(s) used to cover the set A
fBm	fractional Brownian motion
F	Frequency count of the reflected intensity over an area
FD	Fractal Dimension
ϕ_n	arbitrary phases
γ	scaling constant in fBm function
g, v_x	Scattering equation parameters (used for simplification)
G(f)	Spectral density function
H	Parameter defining the fBm

h	Height variation along the trace
I	Incident angle of light
λ	Incident angle of light
μ	Mean of the pixel values in the image
N	Surface normal vector
N(s)	Number of boxes of size s that lie within A
O	Observation vector
$p(B\mid \theta)$	Likelihood of fBm process
$P(\lambda)$	Total spectral power of the incident radiation
$\theta_1,\theta_2,\theta_3$	Parameters describing the facets
Ra	Roughness Average in μm
$\Re E$	Space defined by E number of coordinates
s	Size of boxes that are super imposed on *A*.
$S(\omega)$	Power spectrum of W-M function
T	Statistical correlation distance between peaks on the surface, as defined by Beckmann [BS63]
V(x)	One dimensional W-M function which is used to model the machined profile.
V(x,y)	Two dimensional W-M function, used to model the machined surface.
W-M	Weinstrass Mandelbrot function

$\vec{X}$	Vector with the x,y, and pixel brightness as its components
x	Distance in mm
z(x)	Fractional Brownian function which relates the height of a profile with respect to x.
Z_n	String which holds the number of points in the boxes used to cover the set A.

Chapter 1

Introduction

1.1. Background

On-line process monitoring has been an active area of research as it is recognized as a critical component of a fully automated manufacturing system. Such a system would be essential in the future to produce high quality products without compromising on productivity. Of the many parameters that are to be controlled in the manufacturing of a product, surface finish of the material is an important parameter. The surface finish of a product is a vital criterion in the performance and utility of industrial products.

The degree of control on the surface finish required on a product, determines the machining time of the product. A surface maybe intentionally made rough for special requirements, e.g., knurling. An understanding of the relationship between surface texture and performance properties of the surface can lead to the specification of optimized manufacturing processes for various surface function needs. Also in the global marketplace, with the machining centers located around the world, new parameters are

required to describe the surface topography, so that information can be transmitted worldwide in real time.

1.2. Issues in sensor based manufacturing

Typically, the surface finish is measured manually for a sample in a batch of products, after the machining process. The batch is sent to the next stage of processing, depending on whether the product's surface roughness lies within limits or not. A defective batch may either be scrapped or reworked. This process results in loss of productivity and raw material. Also in general, the sample size in a batch must be increased to ensure high quality. The above method also suffers from the following disadvantages:

- Use of manual operations to perform quality assessment and thus resulting in potential human error.
- Many defective samples may go undetected since only a small number of the total products are inspected.
- Manual interpretation of the inspection results may not lead to optimal increase in product quality and productivity.

In order to overcome these difficulties, active control systems must be used. The machined surface is monitored for surface quality continuously through sensors (pressure, force, temperature, light scatter, etc.). The sensed readings are then interpreted by an expert system and changes in the machining parameters are made accordingly.

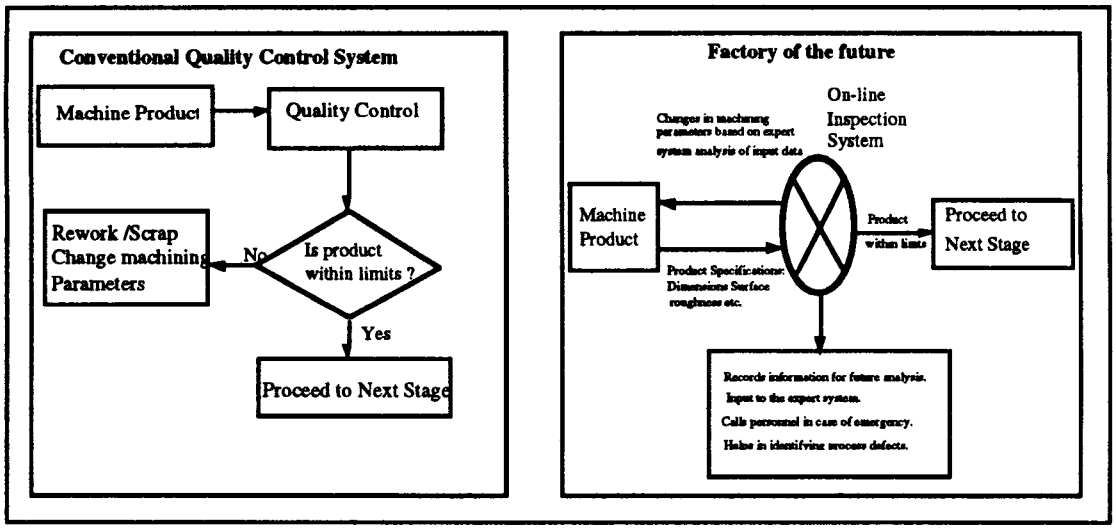

Figure 1.1 Conventional versus future quality control system

Surface roughness of the machined part is an important parameter that is to be measured in many quality control programs. Traditional methods use off-line systems that have inherent disadvantages as described above. Therefore an on-line monitoring system is needed to provide feedback to the control system to keep surface roughness within desired tolerances.

Current surface roughness assessment systems can be divided into three main categories, namely contact profiling techniques, optical techniques and area based techniques [VR90]. Of the above three, only optical methods and area based techniques, like capacitance methods, are more suitable for on line monitoring as they do not involve direct contact with the machined surface [DF86]. Optical techniques may be classified into interferometric, differential scattering and speckle pattern contrast. In essence these methods give an estimate of the power spectral density of the surface roughness. In most of the literature it is assumed that this density is well behaved so that it is possible to find the moments of measurements [LHN89, CHR79, TV57].

Roughness measurements on variety of surfaces show that the power spectra of the surface profiles follow power law [MB90]. This suggests that under appropriate magnification, the magnified image looks very similar to the original image. Mandelbrot, founder of fractal geometry, describes this property mathematically by the concepts of self-similarity and self-affinity [MB82]. Fractal dimension, a scale invariant parameter, can be used to describe self-similarity and self- affinity. Therefore it can be used to characterize surfaces completely and provide geometric structure at all length scales. Fractal geometry provides the means to describe complex geometrical entities by using a small number of coefficients and simple equations.

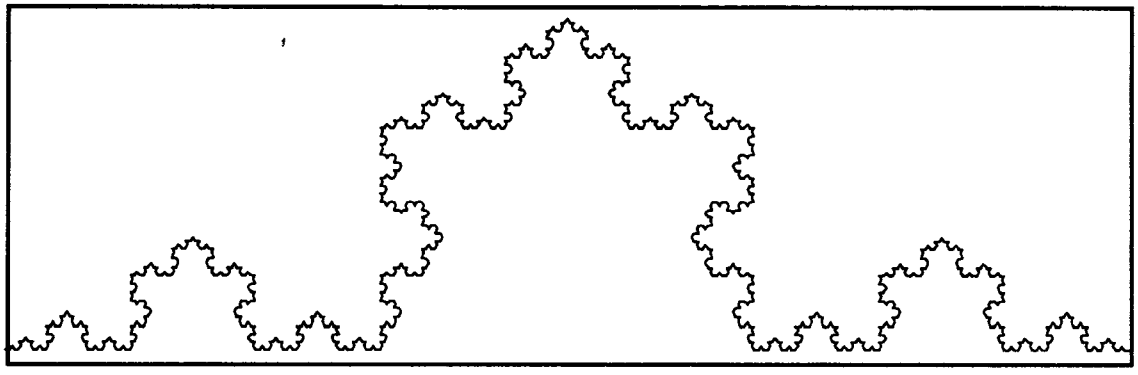

Figure 1.2 Example of a fractal curve - Koch curve

The need for faster surface roughness assessment systems calls for faster algorithms that can be implemented using commercially available hardware systems. Profilometric methods lack the ability to characterize the entire surface as they scan the surface line by line. This slows down the process of surface roughness measurement as it would take many scans to estimate the true roughness over an area. Therefore the new system must be able to access the surface roughness over an area of interest. This would expedite the process of roughness measurement as the surface roughness of the entire region may be assessed, instead of analyzing the surface line by line. The ideal system would have the speed and accuracy of a laser system and at the same time would be able

to characterize the entire region of interest. This is particularly important in milled surfaces as the roughness varies along the milled path. Also the system must realistically model the surface and must not make assumptions that would make the system impractical. The ability to characterize the entire surface in one measurement over an area is very important in accessing the surface roughness of milled surfaces.

1.3. Operation of the developed prototype vision system

A basic description of the system is given without much theoretical background. The theory is explained in the following sections. The aim of this section is to give a basic idea of the proposed system and to bring out the uniqueness of the new system as compared to the techniques described in previous sections.

The optical systems previously mentioned have been concerned with the measurement of reflected light intensity over a full range of reflected angles, or studying the width of the scattered field in the case of infra red systems. The fractal methods, use complex procedures to estimate the fractal dimension that would determine the surface roughness independent of the scale of measurement. Most of the fractal methods use inputs from profilometers thus cannot be used for on line monitoring for reasons mentioned in section 1.2. This vision system examines the brightness levels from a digitized image of the surface. Also the fractal dimension is calibrated against the required scale of measurement. This facilitates the quick calculation of the fractal dimension of the surface. The system consists of a microcomputer, which is used to analyze the image. The image of the surface is obtained through a CCD camera. The sample is illuminated by a white light source through fiber optic cable. The CCD camera provides a video signal,

which is digitized by a frame grabber. The frame grabber has the capacity to convert the image into an 8-bit gray scale digital image at a rate of 30 frames per second. The digitized image is sent for processing by the microcomputer. The computer on receiving the image, plots the surface profile based on the brightness levels of each pixel. From this surface plot, the fractal dimension (FD) of the surface is determined. Since the magnification scale of the camera is constant, the fractal dimension alone can be used to classify the surface roughness. To obtain further distinction among surfaces the lacunarity of the surface maybe calculated. The R_a value is then computed using a correlation curve, which uniquely relates a given value of FD to a R_a value. This can be used as feedback to the control system of the machine tool to update the machining parameters.

The proposed system will be tested on a prototype vision system. The system contains a test stand, a variable intensity light source, a fiber optic cable to orient the incident angle of light, a CCD camera and microcomputer with a digitizer. The Image processing software NIH-Image developed by NIH, is used to analyze the image.

The frame grabber acquires 510x490 pixel image, which reflects the activation levels of the CCD elements in the camera. This 256 gray level image is used to generate the surface plot. The surface plot is then analyzed by a fractal dimension estimator, which is incorporated in the image processing software. This program takes in the surface points as input and computes the fractal dimension. It will be shown that the fractal dimension of the surface is related to the surface roughness. For more accurate description of the surface, if needed, the fractal property known as lacunarity, which is related to frequencies existing in the random surface, can be estimated. A calibration curve is generated by estimating the fractal dimension surfaces with known Ra values. Using this curve the surface roughness of any similar surface can be determined.

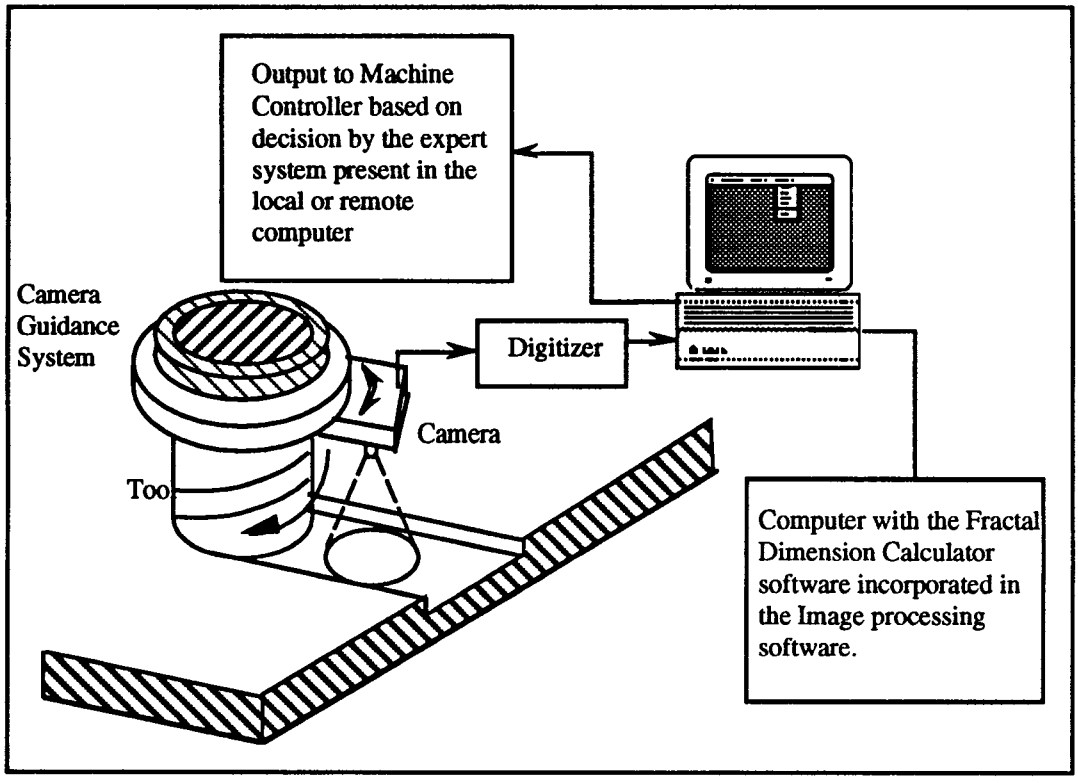

Figure 1.3 Prototype on line surface roughness monitoring system.

1.4. Application of the image processing system in wireless communication

An important application of this method is in wireless communication where bandwidth is very important. In today's global market more and more companies are opening new factories in different regions of the world to reduce the manufacturing costs. One of the main concerns in such a global market is to maintain high quality in the manufactured products. Continuous monitoring is required in such environment to keep up the quality of the products. The factories maybe located in places where conventional communication systems may not be reliable or not present at all. In such an environment, wireless systems provide the solution to the communication problems.

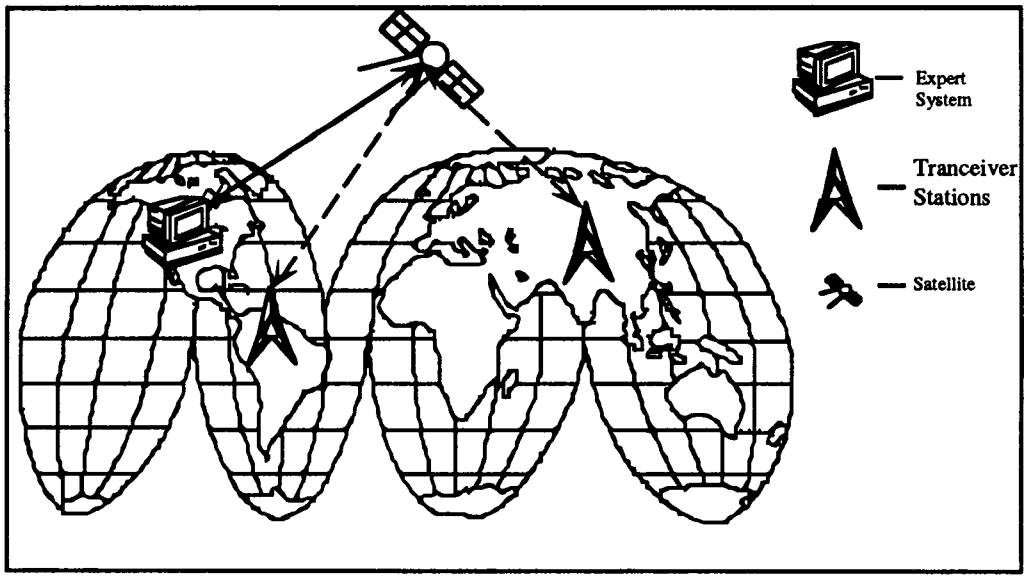

Figure 1.4 Wireless systems linking manufacturing centers around the globe.

Wireless communications are currently being used in manufacturing applications as a tool to monitor the status of the inventory, work in progress, etc. In the future it would also be necessary to monitor the quality of the machined product so that the product is made within tolerances. An expert or an expert system, in a remote location, maybe monitoring many machining operations. The person would require information on the surface roughness. Very often it is necessary to visualize the surface topography of the machined surface, so that an analysis can be made to determine the various parameters that describe the surface topography, e.g., Ra, Rms, Rq, etc. Conventional description methods of surface roughness require a very large bandwidth and therefore not practicable. Knowledge of fractal dimension and lacunarity of the surface can be used to reconstruct the surface. The image processing system will obtain the fractal dimension and the lacunarity of the machined surface. These values are then transmitted to the main computer through a wireless system. The main computer reconstructs the surface using scaling parameters obtained from analyzing surfaces of known topography. Thus this method of analyzing surface roughness can be used to transmit topographical information to distant control centers with minimum bandwidth.

1.5. Organization and scope of the thesis

The thesis is organized into 6 chapters each of which is described below.

Introduction: The importance of monitoring surface roughness is explained. A review of currently available systems is made and the need for the new system is demonstrated. A basic description of the proposed vision system and its theoretical background is given. The future application of the system in wireless communication systems is also presented.

Literature Survey: The light scattering theory and its application in estimating surface roughness is presented. An introduction to fractal geometry is given and the methodology of applying fractal dimension and other fractal parameters to estimate surface roughness is shown.

Vision system description and operation: A basic description of the vision system and the theory behind its operation is given. Also the effect of variables affecting the systems measurement is also described.

Experimental setup and results: The prototype system is put to the test and the effect of various variables on the system is estimated using factorial design of experiments.

Testing of the vision system on the CNC machine: The performance of the system is then tested on the CNC milling machine. The results are recorded.

Conclusions and Recommendations: The results from the experiments are discussed and conclusions are derived. Recommendations are made to improve the performance of the system.

Chapter 2

Literature review

2.1. Terminology and definitions

Fractal geometry is an extension of classical Euclidean geometry. It can be used to accurately represent naturally occurring shapes like the profiles of mountains, surface profiles, clouds, leaves, etc., using a very simple and compact set of equations. Infinite numbers of fractional dimensions are permitted in fractal geometry as opposed to the three integer dimensions allowed in Euclidean geometry. Fractals are identified by their property of appearing similar to the original image under a range of magnification scales. In broad terms, fractal is a rough or fragmented geometric shape that can be subdivided in parts, each of which is nearly a reduced copy of the whole. Fractals can be described by a scale invariant parameter called as fractal dimension denoted by D. Fractal dimension is a measure of how dense the fractal occupies the space in which it lies.

Optical methods use the theory of scattering of electromagnetic waves with the surface irregularities [SM66, SRS82, TTR82]. In particular, the scattering of light waves

on rough surfaces is of interest as it can be used to describe the roughness of surfaces encountered in machining. Beckman [BS63] investigated this phenomenon and his analysis provides the basis for understanding this problem. Though much of this research was motivated for the study of radar interference due to irregularities on the ground, the results are equally applicable to scattering of light waves on rough surfaces. Beckman's theory combined with geometrical interpretation of reflection provides the validity of using the digitized image of the surface as a true representation of the machined surface. Some of the basic terms in electromagnetic reflection is presented before the theory is presented.

The terms 'specular reflection' and 'diffuse reflection' are used to describe the two extremes of the manner in which electromagnetic radiation is reflected of surfaces. Specular reflection occurs as a result of constructive interference between multiple scattered and reradiated waves. Light exhibits purely specular reflection for a given material when the entire light energy is reflected away from the material at an angle equal to the incident angle, as measured from the material's surface. The phase of specular reflection is coherent. In contrast, light exhibits diffuse reflection when the specular direction is not favored over other directions for the reflected energy. The phase of diffuse reflection is incoherent. There is continuous transition from diffuse to specular reflection. In reflection from any real engineering material, a combination of both types of reflection will be present. This fact is used to represent the machined surface in its digitized form.

Since the phase of specular reflection is coherent, the total power density of light waves from specular reflection is determined from the vector sum of the individual waves. In contrast, the incoherent nature of diffuse reflection allows the mean power density of light waves to be calculated from the algebraic sum of the individual mean

power densities. This is true since the phases of coherent waves are constant, while the incoherent waves have random phases. As with specular and diffuse reflection, there is a continuous transition between coherent and incoherent light.

An important effect of light reflection on surfaces is called scattering. Scattering refers to reflection, which is diffuse. Scattering occurs for any surface that is rough, and as it will be shown later, that the amount and nature of the scattering is a function of the roughness of the reflecting material. Diffuse scattering is composed of two components: scattering due to surface waviness much larger than the wavelength of incident light, and scattering due to surface roughness in the same range as the wavelength of incident light. The former component of diffuse scattering is highly directional, while the latter component is essentially isotropic in its scattering.

2.2. Fractal geometry

2.2.1. Introduction to fractal geometry

Mathematicians use Euclidean geometry to describe the properties of objects. They deal with ordered objects such as points, curves, surfaces and cubes using dimensions of 0,1,2, and 3 respectively. Euclid geometry is very helpful in simplifying and approximating complex system to a manageable system. But most naturally occurring geometric features cannot be adequately described by Euclidean geometry. Such objects include the shapes of clouds, mountains, coastlines, etc. All these objects have a common property that under a range of magnification scales they look similar to the original image. Mandelbrot introduced a new kind of geometry to describe these shapes and gave the name fractal geometry [MB82]. The shapes themselves are called fractals. Roughly fractal

is a rough or fragmented geometric shape that can be subdivided in parts, each of which is nearly a reduced size copy of the whole. Also fractal shapes have randomness or chance built into them. It is their property of looking similar under different magnifications that give them a certain order. Fractals are continuos but not differentiable anywhere.

2.2.2. Fractal dimension

Fractals can be described by scale invariant parameter called as Fractal Dimension. Fractal dimensions are numbers, which attempt to quantify a subjective feeling on how dense the fractal occupies the metric space in which it lies. There are two types of fractal dimension, Hausdroff Fractal Dimension and Similarity fractal dimension. Hausdroff dimension is more theoretical and is difficult to estimate practically. But it gives a basic idea of what a fractal dimension is as opposed to the conventional Euclidean dimension of objects.

2.2.3. Hausdroff fractal dimension

Consider a line made of small length segments of length ε. Therefore the length of the line is given by

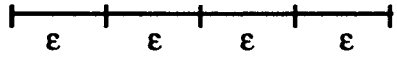

Figure 2.1 Line of length L divided by ruler of division ε

$$L = N \varepsilon^1 \qquad (2.1)$$

where N is the number of segments of length ε needed to fill the line.

Similarly area of a surface can be measured by covering the surface with small squares of dimension ε x ε, and adding the squares together.

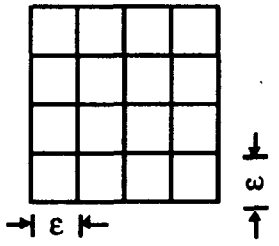

Figure 2.2 Square of area A divided by a grid with side = ε

$$A = N \varepsilon^2 \tag{2.2}$$

again where N is the number of squares of side ε required to fill the square.

From (2.1) and (2.2) it is seen that the exponents of ε, i.e., 1 & 2, correspond to the dimensions of the object. The exponents are unique property of the objects and are independent of the unit of measurement ε, and in the limit $\frac{\varepsilon}{E} \to 0$ these measures remain finite and non zero. The above concepts can be generalized as

$$M = N \varepsilon^D$$

where M is the unit of measure and D is a real number.

Extending the above definition if we assume that an object of unit measure M, is divided into N equal parts, then

$M = N\varepsilon^D$

But M is constant independent of the unit of measure. Therefore $N \approx \varepsilon^{-D}$. If the length of an object, whose dimension is D, is measured then $L=N\varepsilon^D \equiv \varepsilon^{1-D}$. Therefore, only when D=1, the length is independent of the unit of measure. For all fractals, there exists a dimension D, not necessarily an integer, such that any measure M is independent of the unit of measure. The exponent D is known as the Hausdroff Fractal Dimension [BDV88]. This dimension is very difficult to calculate practically, but it gives an idea of what a fractal dimension is.

2.3. Self- similarity

Self-similarity generally means that under different scale of magnification an object looks similar to the original.

2.3.1. Mathematical definition

In Euclidean geometry, $\Re^E$ defines a space, where any point can be uniquely defined by E number of coordinates. Also similarity transformation is defined as a function r(x) such that $x = \{ x_1, x_2, x_3, ..., x_E \}$ will be transformed to $\mathbf{X} = \{ r*x_1, r*x_2, r*x_3, ..., r*x_E \}$.

A bounded random set S, is defined as statistically self- similar, with respect to ratio r, and an integer N, when S is the union of N non overlapping subsets, each of which is in the form of $r(S_n)$ where the N sets S_n are congruent in the distribution to S.

2.3.2. Use of self-similarity

A line of unit length can be broken into equal segments of length $1/\varepsilon$. Each such segment is similar to the original and needs a magnification of ε to be a replica of the original line. The number of such segments $N=\varepsilon$.

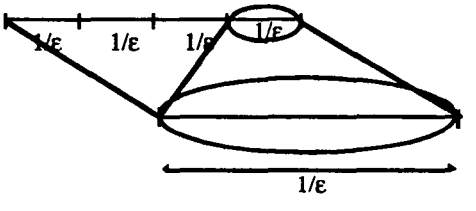

Figure 2.3 A part of a line magnified resulting in the creation of the original line.

Similarly for a square having unit sides, a small square of side $1/\varepsilon$ needs a magnification of ε to be a replica of the original unit square. But the number of squares of side $1/\varepsilon$, inside the unit square is $N = \varepsilon^2$.

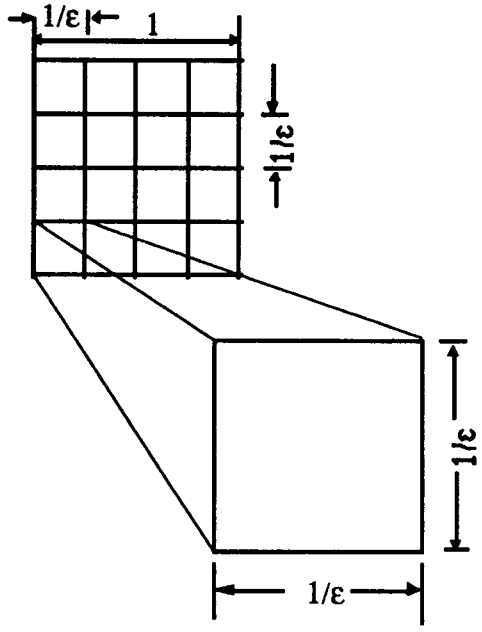

Figure 2.4 Part of the square magnified to create the original square.

Therefore in general, for an object of dimension D, it can be said that

$N \sim \varepsilon^D$

Hence the dimension of an object can be obtained by

$$D = \frac{\log N}{\log \varepsilon} \tag{2.3}$$

This definition of dimension of an object, based on object's self-similarity, is called similarity dimension [MB82].

Koch curve has a similarity dimension D = 1.26, which is a real number. To see how this ratio was arrived the construction method of Koch curve must be known. Koch curve is constructed as follows. Take a straight line and break it into three equal parts. Remove the middle part and replace it with two segments of equal length such that it

forms an equilateral triangle without a side. This process is carried out recursively on each straight length segment. If this process is carried out infinitely Koch curve is obtained.

This curve has some interesting mathematical properties. Even though the curve is continuos it is not differentiable anywhere. This is due to the fact that as the curve is repeatedly magnified more and more details of the curve keep appearing. This implies that a tangent cannot be drawn at any point and the curve cannot be differentiated anywhere. Also the curve is exactly self-similar. That is if the curve is appropriately magnified it will be a replica of the original curve.

If the Koch curve is started with a line of unit length, then L(1) =1. After the first iteration the length increases by 4/3 x 1. After next iteration the length is 4x 4/9. Therefore, in general, each segment length ($\varepsilon/3$), where ε is the original straight line segment, increases by a factor of 4/3. Therefore

$L(\varepsilon/3) = 4/3 \times L(\varepsilon)$

For the above to satisfy the equation $L= \varepsilon^{1-D}$,

$\log 4 / \log 3 = 1.26$

Thus Koch curve has a similarity dimension of D= 1.26, which is not an integer. It can also be shown that Hausdroff dimension is the same for Koch curve. This is a special case and is satisfied by curves that are exactly self-similar. The procedure is illustrated in figure 2.5.

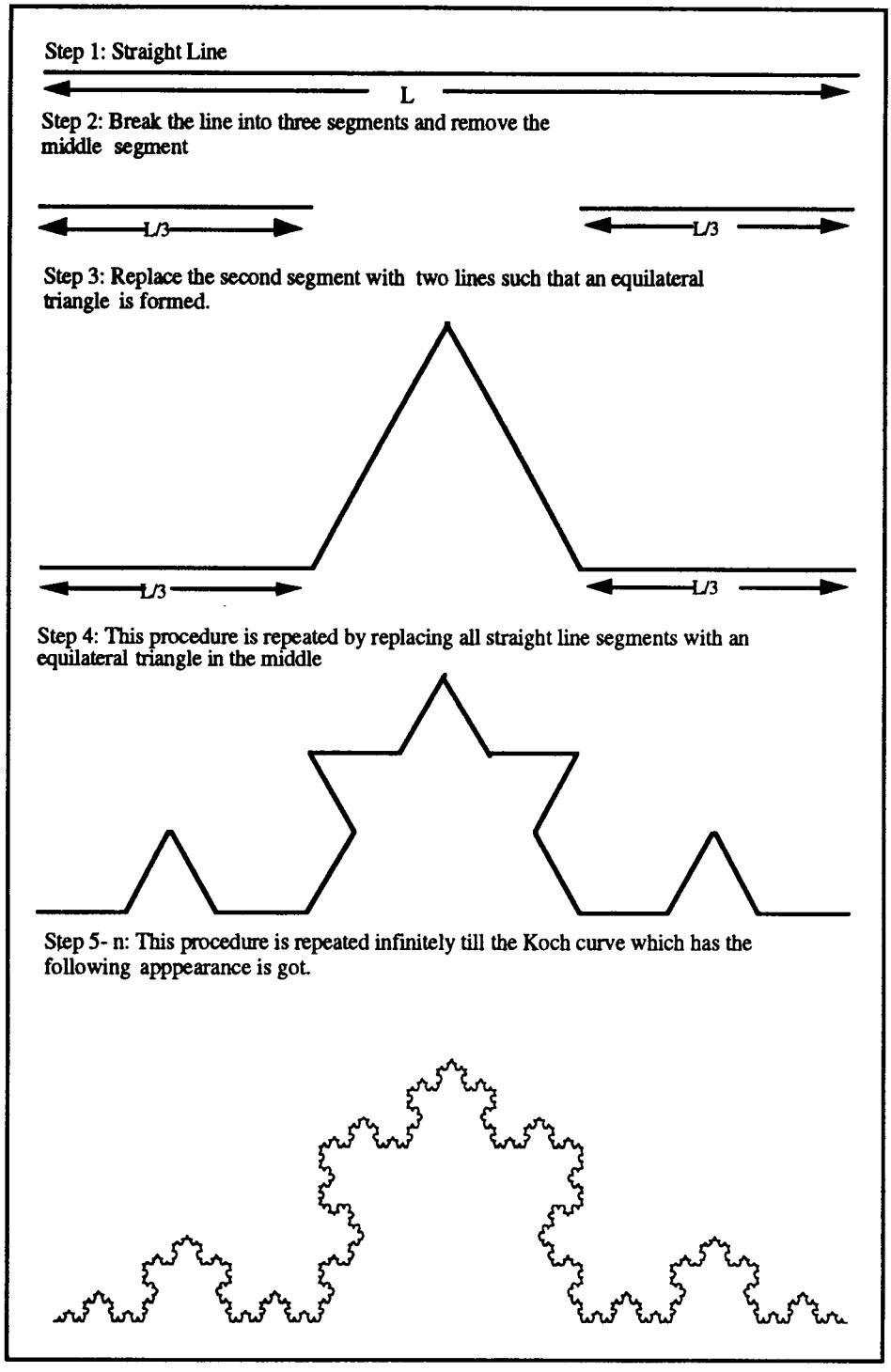

Figure 2.5 Procedure for creating the Koch curve

2.4. Self- affinity

Self-similar curves appear similar under equal magnification in all directions. But there exists some curves in nature that look similar to the original only when magnified under unequal ratios along different directions. Such a curve or surface, which has this property, is known as self-affine curve.

2.4.1. Mathematical definition

In Euclidean space $\Re^E$, affinity transform is defined as a transformation r(x), of a point $\mathbf{x} = \{x_1, x_2, x_3, x_4 ....., x_E\}$ to $\mathbf{X}$ such that

$\mathbf{X} = \{ r_1 x_1, r_2 x_2 ....., r_E x_E \}$.

Similarly a bounded set S is self- affine, with respect to ratio vector $\mathbf{r}$, and an integer N, when S is the union of N non overlapping subsets each of which is congruent to r(S).

The concept is explained below. The first plot shows the height variation (h) versus the position (x). The second plot is obtained by equal magnification on both axes. From the figure it is evident that even thought plot looks similar to the original plot the curve looks elongated along the h direction. However under unequal magnification along h and x axes the third plot is obtained which looks similar to the original profile curve. This property of being similar under unequal magnifications along the axes is called self affinity, and the curves are called self-affine curves. The profiles obtained from the machined surfaces are self affine [LNG90].

2.4.2. Self affinity applied to surface roughness measurement

One of the common examples used to explain self- affinity is curve generated by a particle executing a Brownian motion. Brownian motion is the path taken by finely suspended particle in a liquid. Unlike large objects this particle does not sink but moves in a random motion. This random motion is called Brownian motion. Later it will be shown that Brownian motion is a special case of fractional Brownian Motion as defined by Mandelbrot [MB85].

The curve generated by Brownian motion, is a plot between its location and time. Under equal magnification this curve does not look similar. But under a magnification of γ on the t-axis and $\gamma^{1/2}$ on the position axis this curve looks similar. Thus Brownian function is self-affine.

The above observation can be explained as follows. The statistics of the Brownian function follow the relation [MB85]

$\mathbf{B}(\gamma t) = \gamma^{1/2}\mathbf{B}(t)$ Assuming $B(0) = 0$

where **B** is the probability distribution of B. From the above equation is clear that if time t scales by γ then the position of the particle B scales by $\gamma^{1/2}$. Therefore Brownian motion is statistically self-affine.

From figure 2.6 it can be seen that profiles of rough surfaces follow fractional Brownian motion and are self-affine. Figure 2.7 show striking similarity between the profile obtained through profilometric measurements and the computer generated fractional Brownian motion curve.

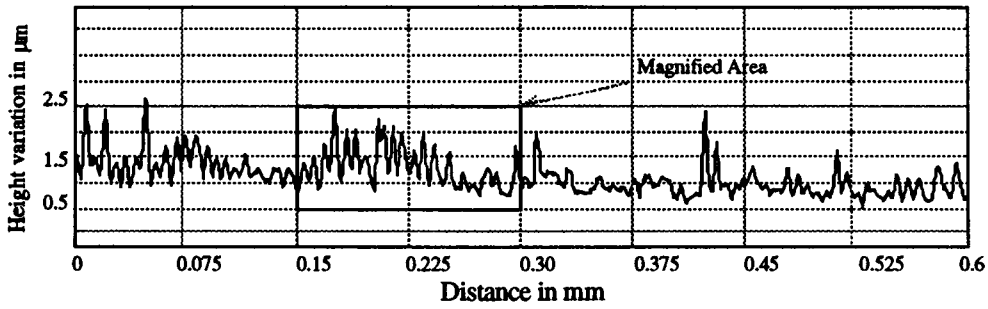

a) Example of a Surface Profile

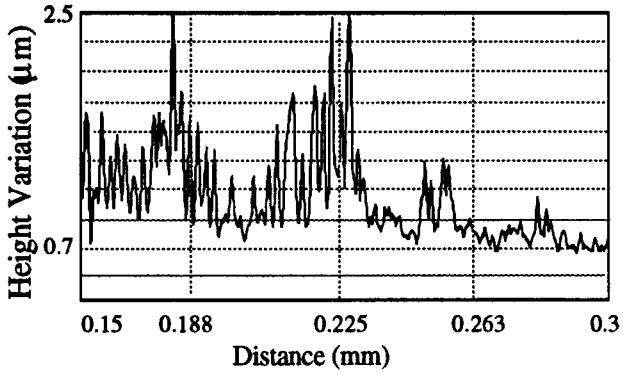

b) x' = 2x and h' = 2h

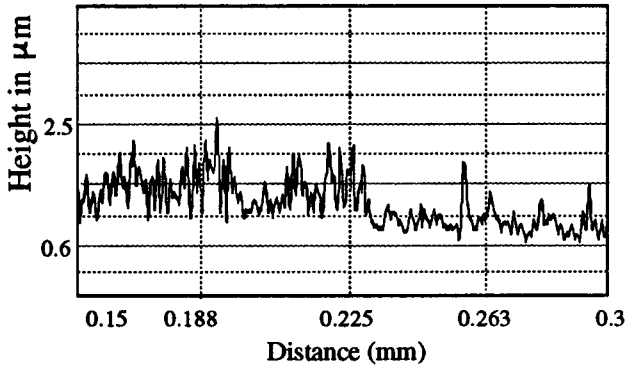

c) x' = 2x and h' = 0.8h

Figure 2.6 Surface profile under different magnification scales on the x and h axes

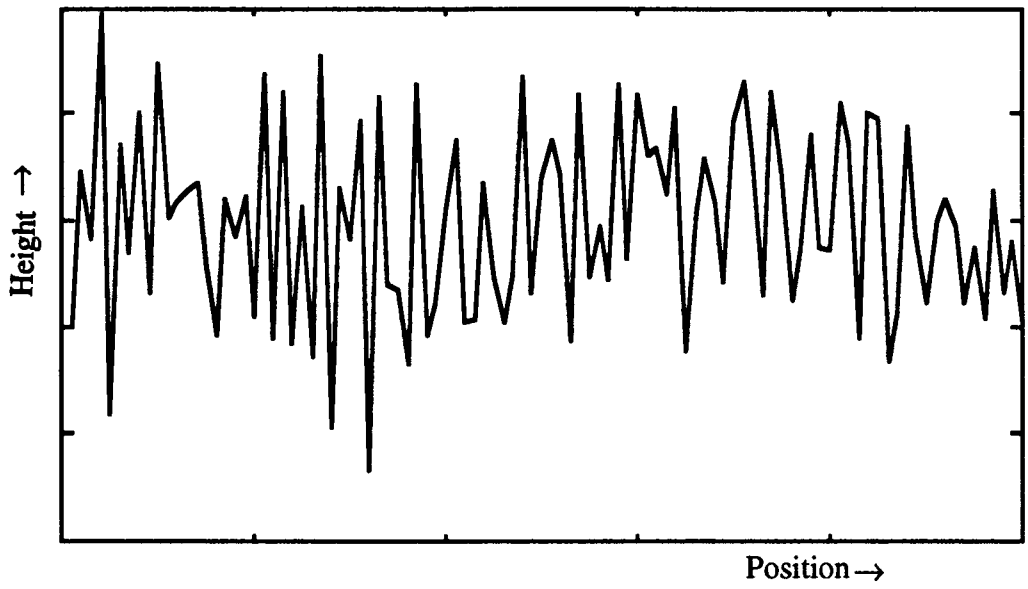

Figure 2.7 Fractional Brownian motion. Height variation versus location (Computer simulation)

2.4.3. Fractal geometry as applied to rough surfaces

Fractal models provide a more realistic representation of description of surfaces, as it is not based on Euclid geometry. The profile of a rough surface z(x) is assumed to be continuous even at the small scales. This assumption is not valid at atomic scales, but for engineering studies the continuum is assumed to exist down to the limit of a zero length scale. It is seen that under increasing scale of magnification more and more details emerge. Therefore a tangent at any point cannot be defined. Thus the profile has the mathematical properties of being continuous but not differentiable anywhere.

2.4.4. Weierstrass - Mandelbrot model for rough surfaces

The Weierstrass - Mandelbrot W-M fractal function was proposed by Mandelbrot [MB82] to model rough surfaces. It is defined in one dimension as

$$V(x) = \sum_{n=-\infty}^{\infty} \frac{(1 - e^{(2\pi j a^n x + \phi_n)})}{a^{n(2-D)}} \tag{2.4}$$

where a = constant >1 related to the lacunarity of the surface.

D = Fractal Dimension.

ϕ_n= Arbitrary phases normally distributed over $[0,2\pi]$.

Extending the above function to two dimensions we have

$$V(x,y) = \sum_{n=-\infty}^{\infty} \frac{(1 - e^{(2\pi j a^n x + \phi_n)} e^{(2\pi j a^n y + \phi_n)})}{a^{n(3-D)}} \tag{2.5}$$

2.4.5. Properties of W-M function

For simplicity, the properties of the one dimensional W-M function (2.4) are discussed below. The properties can be easily extended to higher dimensions by changing all the scalars to vectors of required dimension. W-M function has all the properties of a roughness profile. It is continuous everywhere but nowhere differentiable. Under different scales of magnification more and more details of the roughness appear. So the function is nowhere differentiable. The W-M function also follows the relation

$$V(\gamma x) = \gamma^{(2-D)} V(x)$$

which makes the function self-affine since the scaling for x and V are different.

Although W-M function looks similar to a Fourier series, the main difference between them is that in a Fourier series, the frequencies increase in an arithmetic progression whereas in W-M function they increase in a geometric progression. The

randomness expected in a profile can be generated by choosing a non integer a. This ensures that the phases of the frequency modes in W-M function will never match.

A related function is called a fractional Brownian motion function z(x). z(x) is a single value function of one variable, x, where increments $z(x_2)$ - $z(x_1)$ have Gaussian distribution with variance

$$< \left| z(x_2) - z(x_1) \right|^2 > a \left| x_2 - x_1 \right|^{2(2-D)}$$

where the brackets < > indicates averages over many samples of z(x). Such a function is both stationary and isotropic. All x's are statistically equivalent and the mean square increments depend only upon the difference $|x_2 - x_1|$. It can be shown that fractional Brownian motion is similar to W-M function (MB85).

Fractional Brownian motion (fBm) is most commonly used function to describe and generate fractal surfaces. Many researchers have used in this function to estimate the surface roughness of a profile and to generate the equivalent fractal rough surface.

The fractal dimension of fBm cannot be obtained using the definition of self-similar fractal dimension as the fBm is self-affine. Voss [VRF85] showed that the dimension is related to parameter H by the relation

D = E + 1 -H

where E = number of arguments of the function z(x).

2.4.6. Dependence of surface roughness on fractal dimension

Fractal dimension is being used to determine the roughness in rocks, waves and also to obtain a quantitative description of many naturally phenomena and shapes. As far

as machined surfaces are concerned, Majumdar and Bhushan showed that the power spectra of the surface profiles, obtained from machined surfaces, follow power law. Therefore under appropriate magnification the magnified image of the surface looks very similar to the original surface. This property of an image appearing similar to the original image under different magnifications has been mathematically defined using the properties of self-similarity and self-affinity. These seemingly qualitative properties of the image have been quantified by the use of fractal geometry. Fractals has been shown to have the property and self similarity and self affinity. Fractal dimension of a fractal is an essential property by which a fractal can be described. Therefore using the fractal dimension can be used as a measure of surface roughness.

2.5. Methods of determining the fractal dimension

Currently there are many methods that can be used to determine the fractal dimension of a metric space [V092, LT89, WM93].

2.5.1. Divider method

The divider or the compass method can be described as follows. A divider is opened so that the two points are a distance r apart. The divider is then walked along the profile from one end to the other. The number of steps, N, multiplied by r gives an estimate of the length of the curve, L(r). If the data follow a fractal model then

$L(r) = Fr^{(1-D)}$

where D is the fractal dimension and F is a constant. If log L(r) is plotted as a function of log(r), then the slope of the curve is 1-D.

The two constants F and D fully characterize a fractal model for a surface. The fractal dimension, D, describes how the roughness changes with the scale of observation, while F determines the steepness of the topography.

2.5.2. Spectral method

Spectral methods rely on time series analysis, a long standing and well-established part of applied mathematics. In the spectral approach, amplitude spectra or power spectra are computed from the profile data. Spectral techniques have been developed primarily for the treatment of stationary data. Caution must be used when applying spectral methods to non stationary surface data.

Spectra calculated from ideally self similar or self affine surfaces will have power spectral density functions G(f) of the form

$G(f) = Cf^{-\alpha}$

where f is the spatial frequency and α and C are constants. If log G(f) is plotted as a function of log f, $-\alpha$ will be the slope of the power spectrum. The slope, $-\alpha$, describes how the surface roughness changes with scale, while log C describes the steepness of the surface topography or the total profile variance.

2.5.3. Box counting method

In this method, the curve is covered by boxes of size ε, and the minimal number of boxes required to cover the curve is counted. This process is repeated for boxes of various sizes ε, and each time the minimal number of boxes required to cover the curve is counted. From definitions of self similarity it can be shown that for a fractal

$$D = \lim_{\varepsilon \to 0} \frac{\log N(\varepsilon)}{\log(1/\varepsilon)}$$

where D is the fractal dimension of the surface. So in the plot between log(N(ε)) and log(1/ε), the slope gives the fractal dimension of the curve. The procedure is illustrated in figure 2.8.

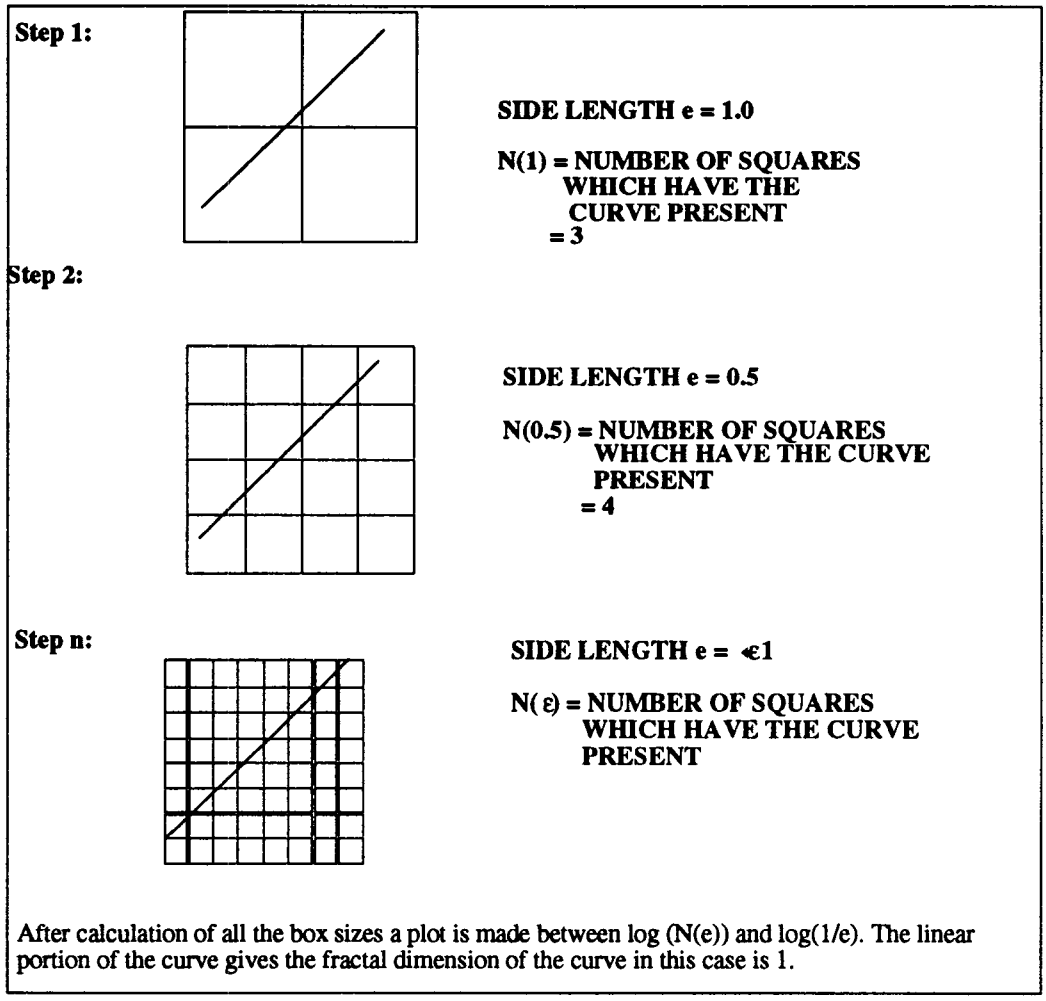

Figure 2.8 Calculation of Fractal Dimension using box dimension method.

Many researchers have put forward theories on using fractal dimension to characterize surface roughness [V092, SA86]. With the above background on fractals we can discuss some of them. In general, all the methods have their own means of estimating the fractal dimension from the surface profiles. These profiles are generated by any

conventional methods. With the fractal dimension the surface profile can be generated and thus all necessary information can be obtained by analyzing the generated figure.

2.6. Surface roughness classifier based on fractional Brownian fractal model

Stephane F. Attali and Fernand S. Cohen [SA86] developed a fractal model to characterize surface roughness using stochastic models. The fractal model has one parameter, fractal dimension. From the single parameter the values associated with that fractal dimension are compared with the values stored in a look-up table. Depending on whether the parameters fall within established tolerance levels the surface is classified as either acceptable or rejected. The system uses the fBm for model-based surface inspection.

2.6.1. System description

The system consists of a feature extractor unit and a classifier unit. The feature extractor unit learns about the surface to be inspected and the features that are used for defect detection. This learning or modeling unit is usually done off-line. The classifier has to perform on-line, to detect whether the product's features are within established limits.

The feature extractor unit is used to extract the distinguishing features from the surface patches. These are the features that are used to determine whether the given surface patch is defective or not. The feature extractor used spatial gray level dependence (SGLD) matrices to model the input texture. The matrices have information on the mean, variance, skewness, etc., of the image of the surface patch.

The (i,j) element of the spatial gray level matrix with parameter (d, q) is the probability p(i, j | d, q) of going from gray level i to gray level j. d is the inter sample spacing and q is the direction.

In general the image is divided into disjoint windows and a maximum likelihood estimate (MLE) for the parameter is obtained. This estimate is compared to a threshold and is determined whether the surface is defective or not.

a) MLE for the fractal model

The field $\{b_r\}$ is described by fBm process. The likelihood of this process is given by

$$p(B|\theta) = (2\pi\sigma^2)^{-N/2}|\det\Sigma|^{-1/2} e^{\{\frac{-(B-\mu)^t \Sigma_{(h)^{-1}} (B-\mu)}{2\sigma^2}\}}$$

where N is the number of samples

$\mu = E[B(x)]$

and σ^2 is given by

$$E[B(x)B(y)] = \sigma^2(\|x\|^{2h} + \|y\|^{2h} + \|x-y\|^{2h})/2$$

where B(x) is fBm process.

The (i,j) element of $\_(h)$ is given by

$$\sigma_{ij} = \{\|b_i\|^{2h} + \|b_j\|^{2h} - \|b_i - b_j\|^{2h}\}/2$$

The maximum likelihood of the fractal parameters (μ, σ^2, h) is now given by

$\mu^* = (\Sigma\, b_i)/N$

$\sigma^{*2} = (b - \mu)^t \sum_{(h)}^{-1} (b - \mu) / N$

with h given by

$$h = \min\left\{ N \operatorname{Log}((b - \mu^*)^t \sum_{(h)}^{-1} (b - \mu^*)) + \log(\det(\Sigma)) \right\}$$

Although the minimization is non-linear and requires an iterative minimizing procedure. But as the covariance matrix is almost Toeplitz it is evaluated using the Levinson routine. Therefore for every h, the matrix is evaluated off-line and stored in a look-up table. Thus the feature extractor unit works.

b) Classifier unit

Now when an image is given as an input to the classifier system, the image is divided into square windows. For each window the SGLD matrix is computed and compared with the one stored in the lookup table. Depending on whether the parameters are within the threshold level the window is classified either as accept or reject.

2.6.2. Working of the system

The system consists of a computer and an image processing system. The samples of acceptable nature are first analyzed by the feature extractor unit. All the surface parameters are computed for different values of h. This is stored in a lookup table. The classifier unit has the basic parameters based on which the system makes the decision. When the image processing system feeds in the image of the surface, the distinguishing features are calculated. This is then compared with the lookup table and decision is made.

Stephane F. Attali and Fernand S. Cohen analyzed different stainless steel surfaces and were able to classify the defective and regular areas on the surface of the plate.

2.7. Fractal geometry used in roughness characterization of surfaces

This method was developed by Majumdar and Bhushan [MB90] to characterize rough surfaces. The methodology is to obtain surface profiles from conventional instruments. From the curve thus obtained, two scale independent fractal parameters, which completely describe the profile, are obtained. The two parameters can then be used to generated the surface profile at any scale and any required statistical property can be obtained.

They use a variation of W-M function to model the surface profile. Let z(x) represent the surface profile. Then

$$z(x) = G^{(D-1)} \sum_{n=n_1}^{\infty} \frac{\cos 2\pi \gamma^n x}{\gamma^{(2-D)x}}; 1 < D < 2; \gamma > 1 \qquad (2.6)$$

where G is the scaling constant

n_1 is the low-cutoff frequency, which is related to the length of the sample by $\gamma^{n1} = 1/L$.

and γ^n are the frequency modes that correspond to the reciprocal of the wavelength of the surface as $\gamma^n = 1/l_n$.

2.7.1. Power spectrum

z(x) is a multiscale function composed of superposition of infinite frequency modes. The power spectrum of the function provides the amplitude of the roughness at all length scales. The power spectrum of the W-M function is given by [BL80]

$$S(\omega) = \frac{G^{2(D-1)}}{2\omega^{(5-2D)}\ln\gamma}$$

From this power spectrum, many relevant statistical parameters can be obtained.

$$\left\langle (z(x_1)-z(x_2))^2 \right\rangle = \int_{-\infty}^{\infty} S(\omega)\left(e^{i\omega(x_1-x_2)}-1\right)d\omega = \frac{G^{2(D-1)}}{(4-2D)\ln\gamma}\Gamma(2D-3)\sin\frac{(2D-3)\pi}{2}|x_1-x_2|^{(4-2D)}$$

$$\left\langle (z)^2 \right\rangle = m_0 = \int_{\omega_l}^{\omega_h} S(\omega)d\omega = \frac{G^{2(D-1)}}{2\ln\gamma(4-2D)}\left(\frac{1}{\omega_l^{(4-2D)}} - \frac{1}{\omega_h^{(4-2D)}}\right)$$

$$\left\langle \left(\frac{dz}{dx}\right)^2 \right\rangle = m_2 = \int_{\omega_l}^{\omega_h} \omega^2 S(\omega)d\omega = \frac{G^{2(D-1)}}{2\ln\gamma(2D-2)}\left(\omega_h^{(2D-2)} - \omega_l^{(2D-2)}\right)$$

$$\left\langle \left(\frac{d^2z}{dx^2}\right) \right\rangle = m_4 = \frac{G^{2(D-1)}}{2\ln\gamma(2D)}\left(\omega_h^{(2D)} - \omega_l^{(2D)}\right)$$

$$\left\langle z(x_1)z(x_2) \right\rangle = m_0 - \frac{G^{2(D-1)}}{(4-2D)\ln\gamma}\Gamma(2D-3)\sin\frac{(2D-3)\pi}{2}|x_1-x_2|^{(4-2D)}$$

The above equations provide the variances of the height, slope and the curvature respectively, between the frequencies of w_l and w_h. The values can be obtained by conventional surface profile measurements.

If the length of the sample and the resolution of the instrument are known, the fractal dimension D and the scaling parameter G can be found. Thus the surface profile is characterized by two scale invariant parameters. Now the surface profile at any length scale can be generated and analyzed.

2.7.2. Measurement procedure

The actual measurement process is done as follows. The instrument parameters like the resolution of the instrument, and the length of the sample are noted. Then surface

The actual measurement process is done as follows. The instrument parameters like the resolution of the instrument, and the length of the sample are noted. Then surface profile of the machined part is obtained. From the surface profile the power spectra of the curve is obtained. Using the slope of the power spectrum the fractal dimension D is determined. The scaling parameter is determined using the instrument parameters.

Now using the fractal surface parameters the profile is generated and analyzed. The advantage of this method is that the results of the analysis do not depend on the resolution of the instrument. Also the parameters provide characterizing parameters for the different surface processing techniques. But this process is time consuming and requires calculation from the surface profile obtained from contact or laser profilometry.

2.8. Surface categorization

Any engineering surface has three main characteristics, which is used to apply Beckman's scattering theory, namely the periodicity, effective roughness, and dimensionality of a given surface.

2.8.1. Periodic vs. random surfaces

Treatment of surfaces with periodic roughness, as encountered in turning, are substantially simpler to analyze than random surfaces. Unfortunately commonly machined surfaces, milled or ground, are essentially random in nature. This work is based on the assumption that the surface is random in nature.

2.8.2. Roughness criteria

A surface can be considered optically rough or smooth on the basis of the Raleigh criterion, which uses a simple light ray model to describe the relationship between the wavelength of the incident light (λ), the angle of incidence (γ), and the surface roughness (h). Consider two light rays incident on a surface with a step discontinuity of height h as shown in the figure. The light ray striking the lower step experiences a path difference of $\Delta S = 2h \sin\gamma$ compared to the second light ray, which strikes the upper step. Assuming that the incident rays are initially in phase, the path difference between the rays results in a reflected phase difference dictated by equation.

$$\Delta f = \frac{2\pi}{\lambda}\Delta S = \frac{4\pi h}{\lambda}\sin\gamma$$

If there is no phase difference between the reflected rays, then the total reflected energy is imply the algebraic sum of the incident rays, directed entirely in the specular direction. Under this condition, the surface is smooth (h=0). As the step height increases and the phase difference approach π, then the energy reflected in the specular direction approaches zero, due to the phase cancellation between the rays.

Surfaces can be classified as one dimensional or two dimensional depending on whether the correlation distance is much smaller than the correlation distance in the perpendicular direction. One dimensional surfaces scatter light similar to radiation emitted from a length of a wire, while two dimensionally rough surfaces scatter light similar to that emitted by a point source.

2.9. Current optical systems

A number of optical systems are commercially available at present, to measure surface roughness [DM85, ZVM89, BGT85]. The systems can use simple desktop systems to complex laser-array systems. A coherent light source, e.g. laser is used in nearly all systems to illuminate the surface, and light sensors are used to examine the reflected light intensity at different points around the surface.

Optical techniques may be classified into interferometric, differential scattering and speckle pattern contrast. In essence these methods give an estimate of the power spectral density of the surface roughness [BD81, GV86]. The optical profiling techniques are the most widely used optical surface roughness measuring systems. They employ optical sectioning or interferometry and focus detection to estimate surface roughness. But these methods generally employ methods that are not very suitable for in - process inspection.

Area based optical techniques use light scattering theory to estimate the surface roughness over a given area of interest. From the light reflected from the surface either empirical or direct theoretical relationships are made between the reflected light intensity and the surface roughness of the machined part.

Chapter 3

Vision system description, theory and operation

3.1. Fundamentals of operation and system components

As seen from the literature survey there are many theories that use fractal geometry to characterize surface roughness [V092, MB90]. These theories are not suitable for on line measurement of surface roughness for the following reasons. The existing theories use large and expensive equipment, which cannot be readily attached to a machine tool. Even if their classifying system is built to accommodate smaller image acquisition systems, their algorithms use too much processing time that the systems cannot be used on a real time basis. Also most of the present theories require that the fractal surface be generated to estimate various parameters of the surface profile. This process is computationally intensive and thus cannot be used practically. The proposed system should overcome all the above handicaps and be able to actively measure surface roughness.

3.2. Basic description of the proposed system

The system consists of a microcomputer, which is used to analyze the image. The image of the surface is obtained through a CCD camera. The sample is illuminated by a white light source through fiber optic cable. The CCD camera provides a video signal, which is digitized by a frame grabber. The frame grabber has the capacity to convert the image into an 8-bit gray scale digital image at a rate of 30 frames per second. The digitized image is sent for processing by the microcomputer. The computer on receiving the image, plots the surface profile based on the brightness levels of each pixel. From this surface plot, the fractal dimension (FD) of the surface is determined. For the prototype system, to test the validity of the fractal model only fractal dimension of the surface is calculated by the program. The R_a value is then computed using a correlation curve, which uniquely relates a given value of FD to an R_a value. This can be used as feedback to the control system of the machine tool to update the machining parameters.

The proposed system will be tested on a prototype vision system. The system contains a test stand, a variable light intensity light source, a fiber optic cable to orient the incident angle of light, a CCD camera and microcomputer with a digitizer. The Image processing software Image developed by NIH, is used to analyze the image.

The frame grabber acquires 510x490 pixel image, which is proportional to the activation levels of the CCD elements in the camera. This 256 gray level image is used to generate the surface plot. The surface plot is then analyzed by a fractal dimension estimator. This program takes the surface profile points as the input and computes the fractal dimension using "box-counting" algorithm. The prototype system is illustrated in figure 3.1 shown along with the photograph of the system in figure 3.2.

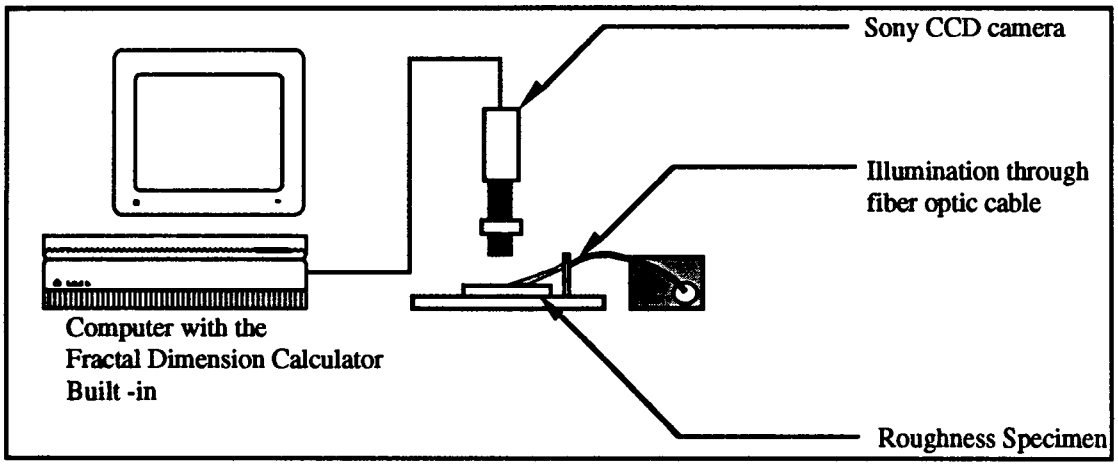

Figure 3.1 Schematic of the prototype vision system

Figure 3.2 Photograph of the prototype vision system

3.3. Application of fractal geometry to vision system components

The theory of fractal geometry and geometric interpretation of incoherent light reflection is used to explain the theoretical basis of the proposed system. Fractals are used to model the surface topography. Properties of fractals are used to describe the rough surfaces encountered during machining of the surface.

As described in the literature survey, a plane surface has a fractal dimension of 2 and cube has a fractal dimension of 3. The fractal dimension of a surface becomes three when the surface occupies an entire volume. Therefore the fractal dimension varies from two to three for all surfaces. The fractal dimension is an indicator of the intuitive perception of surface roughness. The concept behind the analysis of the image to obtain the fractal dimension is as follows. The image of the surface is obtained by the image processing system. From the image a surface plot is generated based on the brightness level of the pixel. On the surface plot boxes of various sizes ε, ($\varepsilon \rightarrow 0$) are superimposed on the surface plot and the minimal number of boxes $N(\varepsilon)$ that contain the curve are counted. The slope of the plot between $\log(N(\varepsilon))$ and $\log(1/\varepsilon)$ gives the fractal dimension of the surface. The above mentioned steps are not carried out physically as the process would be computationally intensive.

A fast algorithm, which implements the above procedure (box counting) is used to determine the fractal dimension. The fast algorithm for analysis of digitized images uses an efficient hashing to code all the points within one box and then to count the number of distinct values.

A vector $\vec{X}$, with components $\{X_i, i=1,d_e\}$, where d_e (=3 here) is the embedding dimension of the set, is used to represent each of the N points of the set.

The values of X_i are normalized to cover the range $(0, 2^{k-1})$, where k (=16 in Mac IIci) is the number of bits required to store an integer (varies with the computer system). The set is covered by the grid of d_e dimensional cubes of edge size 2^m, $0 \leq m \leq k$, called boxes. For each coordinate X_i, $Y_i = (X_i \text{ AND } M)$ where AND is the binary conjunction of the corresponding bits in X_i and M, and M is binary number with 1's in the first (k-m) places and 0's the remainder, is calculated. Then for each n=1, ..., N,

$$Z_n = Y_1 + Y_2 \ldots + Y_{de} \tag{3.1}$$

where the operation "+" indicates concatenation (for example, "01" + "10" = "0110") is done. All the points within the same box 2^m will have coordinates that have identical binary digits in the first (k-m) places. Thus, distinct Z_n correspond to points in distinct boxes. Using an efficient sorting algorithm, such as quick sort or heap sort, all N strings Z_n, is ordered. The list is then analyzed to find the number of times the values of Z change to a different value. The procedure is then repeated for different boxes of edge size 2^m, where m=k,k-1, ... ,0.

The memory space utilized by this algorithm is determined by the number of data points and not the number of boxes in the grid. The computational time required for this analysis depends mostly on the time required by the sorting algorithm, which is approximately of the order N log N steps. So the algorithm is a fast and accurate method of computing the box dimension of the surface. This algorithm is made faster by using binary operations. If the high to low ordering of the bits in Z_n is the cyclic ordering of the bits in the coordinates Y_i, then the Z_n need to be sorted only once for all box sizes. Then for each box size, the box size dependent masking is performed, and the list of Z_n is searched for distinct numbers.

The above algorithm is incorporated in NIH-Image source code and compiled using Think Pascal on Macintosh IIci. To reduce the computational time further only box sizes needed for linear fit of the data were calculated. The ranges of the box sizes

are determined by analyzing the sample specimens of known surface roughness. The slope of the plot gives the fractal dimension of the surface.

3.4. Phenomena affecting vision system performance

In order to apply light scattering theory to estimate surface roughness, several considerations must be taken into account. The two main considerations are shadowing and multiple scattering. The shadowing effect is dependent on the angle of incidence. If the angle of incidence is too small for a given surface roughness, some of the valleys on the surface will be shadowed by the higher peaks. The second consideration is the phenomenon of multiple scattering, which occurs when light scattered from one region of the surface strikes a second region, where it is scattered again. Both of these phenomena affect the measurement accuracy of the vision system.

Shadowing:

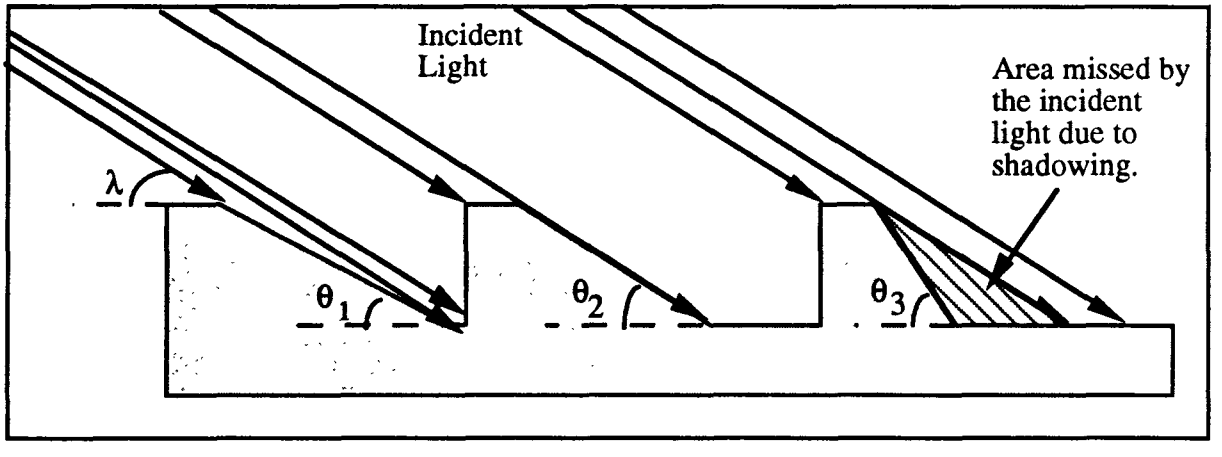

Figure 3.3 Effect of shadow on the vision system

The effect of shadowing is illustrated in the figure 3.3. As seen from the figure, some of the valleys on the surface will be shadowed by the higher peaks if the angle of incidence is too small. This effect does not depend on the roughness of a surface per se, but rather on the slopes of the roughness elements on the surface. If the slopes are steeper than the incident angle, then shadowing will occur. In this figure, the incident light hits the surface with an incident angle λ. The surface is characterized by three distinct slopes of angles $\theta_1 < \lambda$, $\theta_2 = \lambda$, and $\theta_3 > \lambda$. The areas of the surface indicated with the heavy lines are shadowed. As evidenced by Fig. 3.6, shadowing occurs when the surface slope is larger than the incident angle, with $\theta = \lambda$ being a critical angle where shadowing is initiated.

One result of shadowing is that the surface may appear smoother to the vision system. This will affect the representation of the machined surface, and the estimated fractal dimension would be lower than the real fractal dimension if it was obtained through surface profilometers. For this reason, the incident angle used in the system should be large enough to avoid significant shadowing effects.

Multiple Scattering:

Multiple scattering occurs when the incident light is reflected from one section of the surface, and the reflected light strikes a second region of the surface where it is scattered again, and so on. Multiple scattering is most likely to occur when the surface slopes are relatively large, since the scattered radiation is more likely to be reflected away from the surface when the surface slopes are small, thus limiting the effects of multiple scattering. Since it is extremely complex to describe the scattered field reflected from a surface under multiple scattering, the effects of this phenomenon can best be determined through empirical observation rather than from a mathematical description.

3.5. Application of scattering theory to vision system components

From discussion in the introduction it was found that a non contact method is preferred for the analysis of surface roughness. Measurements that involve the use of light probes make assumptions concerning the ratio of the rms roughness to the wavelength of the incident light. Scattering theory can be directly applied to single point measurement systems, but it does not lend itself directly to area based optical measurement

The theoretical basis for the operation of the system with respect to the correlation of surface topography and scattering of light from the surface involves geometric modeling of the surface and application of scattering theory of light [DEV93, BM89]. For two dimensional analysis of the surface, we can model the surface as being made of a series of multi-angled, flat facets as shown in figure. These facets are interconnected to form the overall surface topography. Further the model can be enhanced by considering each facet to have a 'local roughness'. The 'facet geometry roughness' and 'local roughness' must be defined.

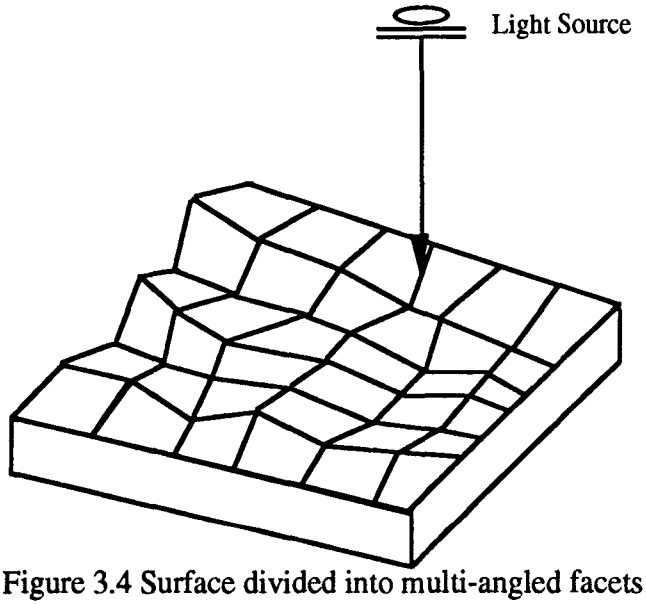

Figure 3.4 Surface divided into multi-angled facets

A small ray cluster of light directed at a single facet of the above model, will be reflected according to the incident angle and global orientation of the facet. In addition, due to the local roughness of the facet, some of the incident radiation is scattered away from the specular direction. In a surface composed a large number of individual facets, the reflected intensity field of light directed from each facet of the surface.

Consider a portion of a surface divided by the facet model and illuminated by a distant light source as in figure 3.4. When a light ray comes in contact with the surface of a facet, much of the incident radiation is reflected away from the surface along the specular direction, which is defined by an angle equal to the incident angle as measured from the surface normal at the point of incidence. If the imaging system is located above the facet, the intensity of the light entering the system, would depend on the vertical component of the reflected radiation. Three vectors are shown in the figure for each light ray: incident radiation, specular direction and the upward directed component of the scattered field. As shown in the figure 3.5, the projected light intensity gradient does not provide a realistic representation of the actual surface. The maximum occurs where the specular and the upward directed component are coincident. For the vision system the facet, which is at the maximum height, appears to be at a lower postion due to the non coincidence of the vertical component and the specular component. The minimum recorded by the vision system occurs at the lowest point of the surface as expected.

The above example shows that the scattered light intensity does not necessarily correlate directly to the geometry of the illuminated surface. Although there is no direct relation, the effectiveness of the optical system is validated by the presence of unique relationship between the surface geometry and the scattered field. The relationship must take into account the slopes of the roughness elements across the surface. Also the relationship must be in a quantifiable form. The integrated scattering surface facet

reflection model is combined with the knowledge of facet orientations to provide a mathematical model of scattering light field.

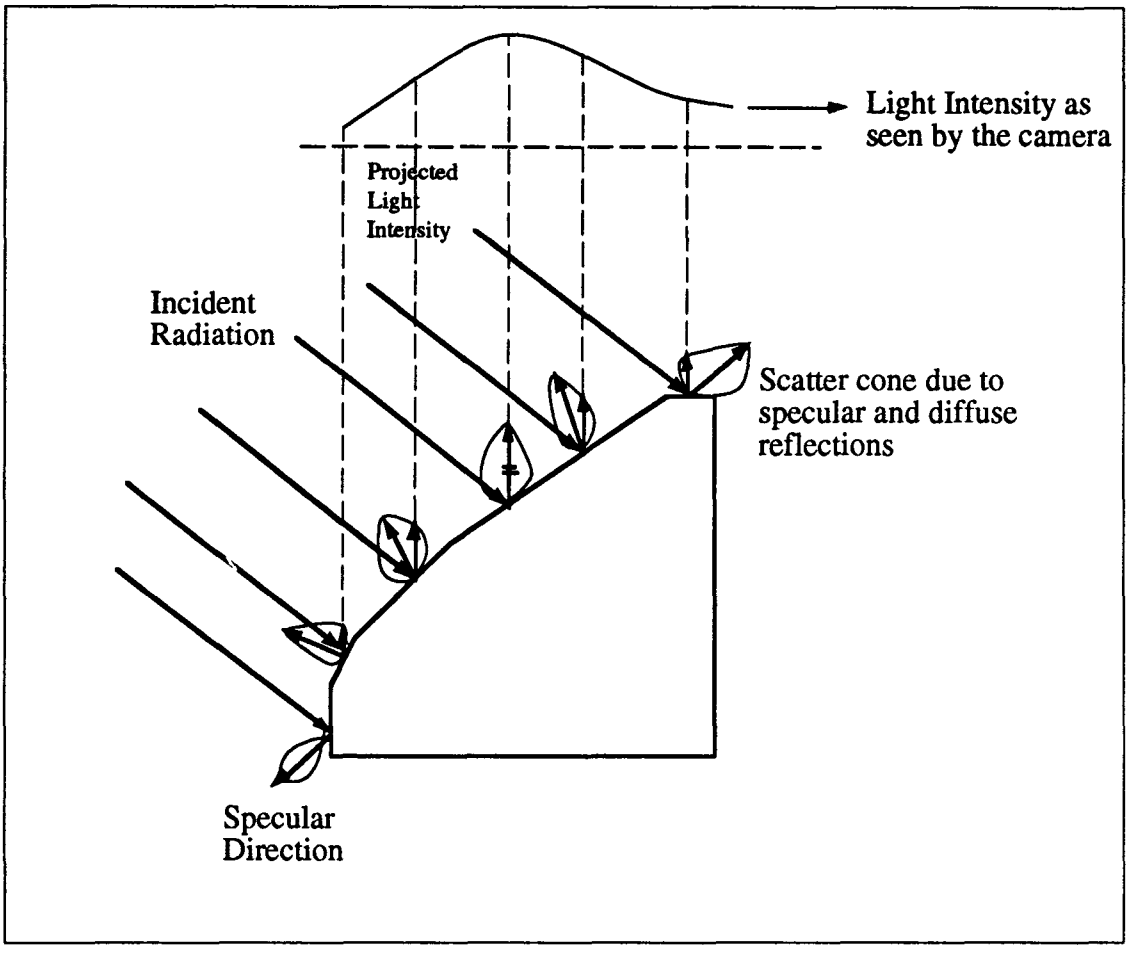

Figure 3.5 One dimensional view of projected intensity over faceted surface

A two dimensional continuous surface can be modeled as a series of discrete surface facets, each with some given local roughness. It is illustrated in the figure 3.6. One such facet, magnified from the continuous surface, shows the local roughness and the geometrical parameters, which define the facet orientation. The surface normal, N, is shown with respect to the mean level of the facet's surface height variation. The incident and observation vectors, I and O, are shown at angles θ_1 and θ_2 from N. The direction of O is dictated by the location of the receiver in the vision system (+Z direction). In

addition, the global angle of incidence, θ, indicates the orientation of I with respect to the global horizontal. Given a fixed incidence angle, the geometric parameters θ_1 and θ_2 are defined with knowledge of the surface facet's normal vector. Extending the figure into three dimensions, knowledge of the facet's normal vector would provide the parameters θ_2 and θ_3, where θ_3 describes the tilt of the observation vector in the third dimension, just as θ_2 describes the tilt in the second dimension. Referring to the scattering equation, we see that the intensity of the scattered field in the known direction of observation can be determined for a given θ_2 and θ_3 in addition to information about the local surface roughness of the facet. Thus, if the surface normal vector is provided for a given facet, and the local surface roughness and the correlation distance of the facet is also known, then the mean scattered power toward the overhead vision system can be calculated for each individual facet of the surface.

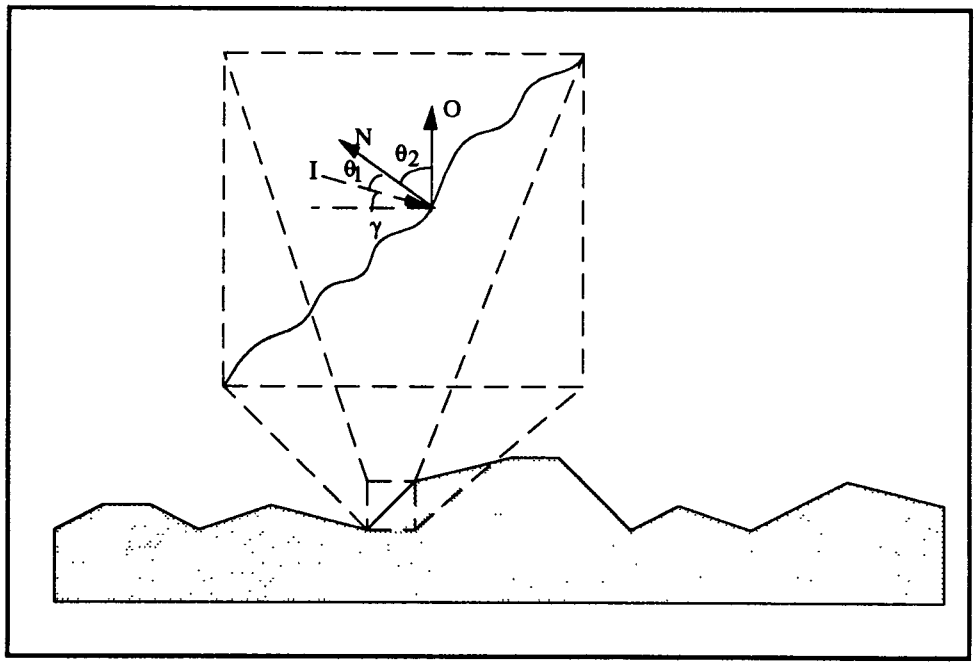

Figure 3.6 Reflection under facet model

In order to determine the mean scattered power from a particular facet, the scattering due to each wavelength of incident radiation must be calculated, and the

resulting scattered field determined by the superposition of the scattering due to each wavelength. To do so, a new term must be provided to describe the relative contribution of each wavelength to the overall incident radiation power, since the light source used to illuminate the surface does not have constant power across the visual spectrum. The function C(λ) is introduced to represent the ratio of the power from a particular wavelength to the total spectral power of the incident radiation, as shown in equations below.

$$C(\lambda_n) = \frac{P(\lambda_n)}{\int_{\lambda_{min}}^{\lambda_{max}} P(\lambda)d\lambda} \tag{3.1}$$

$$\int_{\lambda_{min}}^{\lambda_{max}} C(\lambda)d\lambda = 1 \tag{3.2}$$

The scattering equation can be integrated over the incident spectral range, resulting in,

$$\Psi_{i,j,\frac{\pi}{2}} = \int_{\lambda_{min}}^{\lambda_{max}} \left\{ C(\lambda)\exp(-g_{i,j}(\lambda)) \left[\rho_{o_{i,j}}(\lambda) + \frac{\pi F T^2}{A} \sum_{m=1}^{\infty} \frac{g_{i,j}(\lambda)}{m!m} \exp\left(\frac{-v_{xy}^2 T^2}{4m} \right) \right] \right\} d\lambda \tag{3.3}$$

where λmin and λmax are the lower and upper limits of the spectrum to which the optical receiver is sensitive. Note that the equation (3.3) assumes that the global incident angle (γ) is constant over the full illuminated area of the surface, which is not entirely true for the vision system at hand, since the light source is not distant enough from the surface for the incident light rays to be considered entirely parallel. However, this fact can be overlooked for the current approximation to the scattered field.

The equation (3.3) dictates the scattered power in the observation direction for a given facet defined by the i, j subscripts. This assumes that the facets can be identified in terms of a two-dimensional n x m grid, where i and j are integers such that 1<i<n, and 1<j<m. This notation is convenient, as will be shown in the following discussion of appropriate surface facet dimensions. The parameters, which appear in equation (3.3)

are calculated with θ_2 and θ_3 defined with the observation angle towards the vision system's CCD camera, and defined with respect to the local x-y plane.

In order to apply the equation (3.3), appropriate dimensions for the facets must be chosen such that the continuous surface can be accurately modeled. For the present application, there is a relatively simple choice for facet dimensions. The CCD camera used in the vision system has a resolution of 510 x 492, with each pixel in the camera receiving an amount of light reflected into the camera from a small area of the surface. It is reasonable, then, to model the surface as a 510 x 492 grid of interconnected facets, with each facet scattering the light incident on the facet into a corresponding pixel in the CCD camera. This is reasonable so long as the surface area covered by each facet is small enough compared to the global roughness of the surface. That is, the camera magnification and resolution must be sufficient so that the area of the surface, which scatters light into an individual CCD pixel is smaller than about 1/2 the lower cutoff period of the global surface roughness. Using this 1/2 period criterion assures that the upper cutoff frequency of the continuous surface is modeled by the facets. In summary, the result given by equation rests on the assumptions that the global incident angle is approximately constant over the full area of the surface under inspection, the camera magnification and resolution are high enough so that the surface facet dimensions are smaller than 1/2 the lower cutoff period of the global surface roughness, and that the facet dimensions are large relative to the wavelengths in the spectrum of incident radiation.

Chapter 4

Experimental setup and results

4.1. Preliminary study

The theoretical study of the vision system was presented in chapter 3. The practical implementation and testing of the system are presented in this chapter. A preliminary study is done to examine the basic attributes of the proposed system.

As a first step, profiles of surfaces obtained from the vision system was analyzed using a fractal dimension calculator. The results from the analysis will provide evidence on whether the surface can be modeled as a fractal surface.

Figure 4.1 shows the variation of fractal dimension with the surfce roughness of the profile. It is seen that there is a correlation between the Ra and fractal dimension of the surface. Thus the machined surface can be modeled as a fractal.

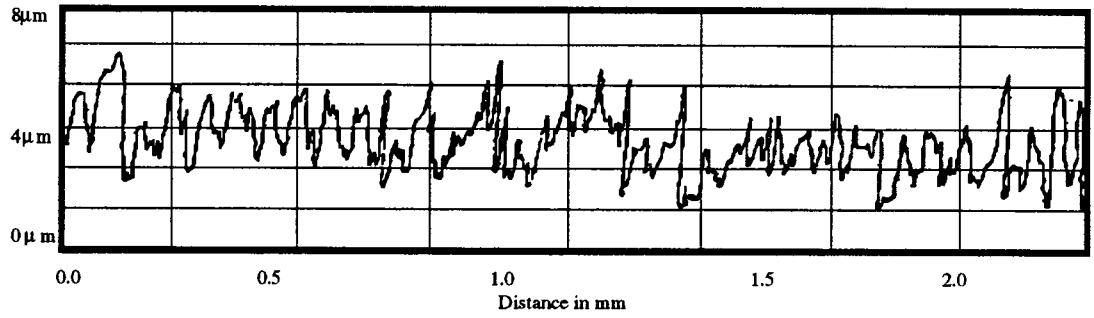

(a) Ra = 0.7µm D = 1.42

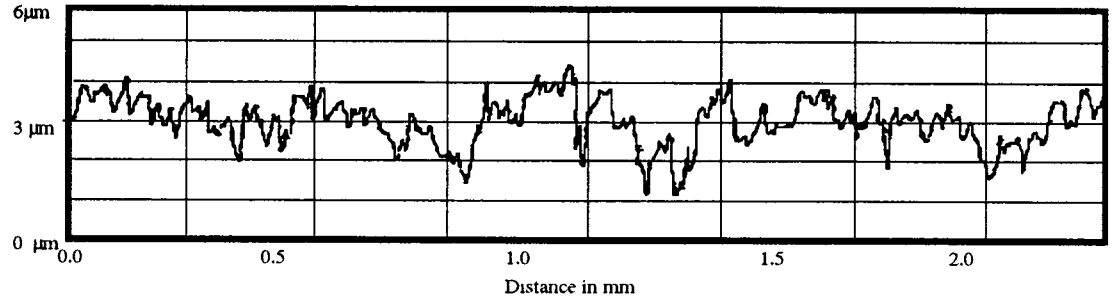

(b) Ra = 0.53µm D = 1.34

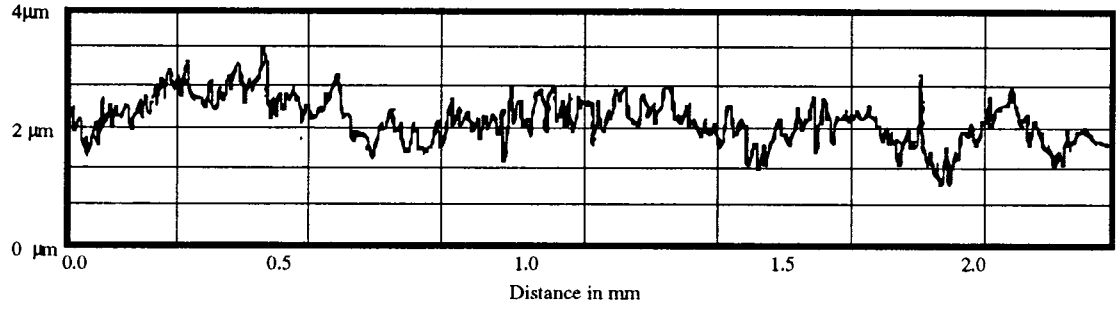

(c) Ra = 0.36µm D = 1.29

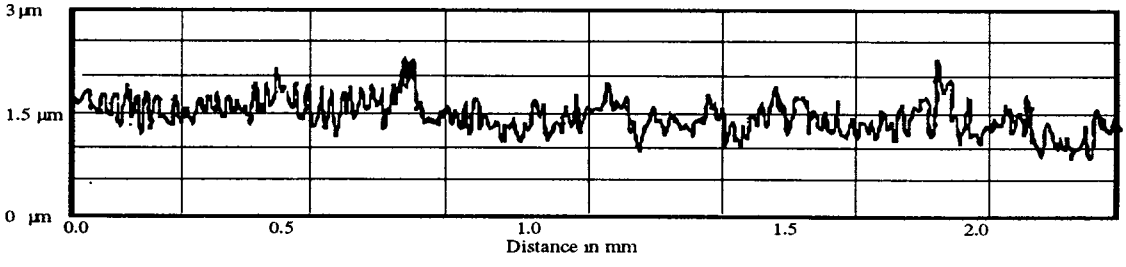

(d) Ra = 0.23µm D = 1.21

Figure 4.1 Variation of fractal dimension with respect to the surface roughness of the profiles

4.2. Preliminary analysis of machined surfaces

The previous study established the validity of modeling the machined surface as a fractal. But the program used is extremely slow and thus cannot be used for on line monitoring. The algorithm described in chapter 3 is a faster implementation of the box counting method. The algorithm was implemented on UNIX mainframe using C language for testing purposes. The testing of the program and its effectiveness in estimating the surface roughness was done using five samples of aluminum, labeled 1 through 5. The samples were prepared under different machining parameter settings to produce different surface roughness.

The image of each sample was stored in the computer, using a SONY CCD camera. The result was an image file with 256 gray levels and of 510 x 490 pixels. Direct lighting was used to illuminate the surfaces. Using a fractal dimension calculating program written in C, implemented on a mainframe UNIX system, the images were analyzed using the algorithm described in chapter 3.

The calibration data was thus data obtained to produce the desired calibration correlation curves. Facilities at the metrology division of the National Institute of Standards and Technology (NIST) were used to measure the sample surface roughness. A Perthometer stylus device was used to calculate the average roughness index, Ra, for each sample averaged over multiple measurement trials.

The numerical data obtained from both the stylus measurement and optical inspections were then plotted to obtain a correlation curve. The experiment proved definitely that a correlation exists between the surface roughness and the fractal dimension of the image of the surface. However variations from the ideal values were observed across the individual samples. These variations are due to the nature of the

machining process employed to produce the samples. Therefore the Ra data observed represents the mean level of Ra for a given sample. The variation of Ra across each sample can be observed qualitatively in the 3-dimensional constructions of the sample surfaces produced using NIH-Image. These images were created by plotting the brightness level of the scanned image along the z-axis, with the sample spatial coordinates in the x-y plane.

Machining Parameters	Sample 1	Sample 2	Sample 3	Sample 4	Sample 5
FEED RATE	1.0	1.2	1.4	1.8	2.0
SPINDLE SPEED	900	900	900	1100	1100

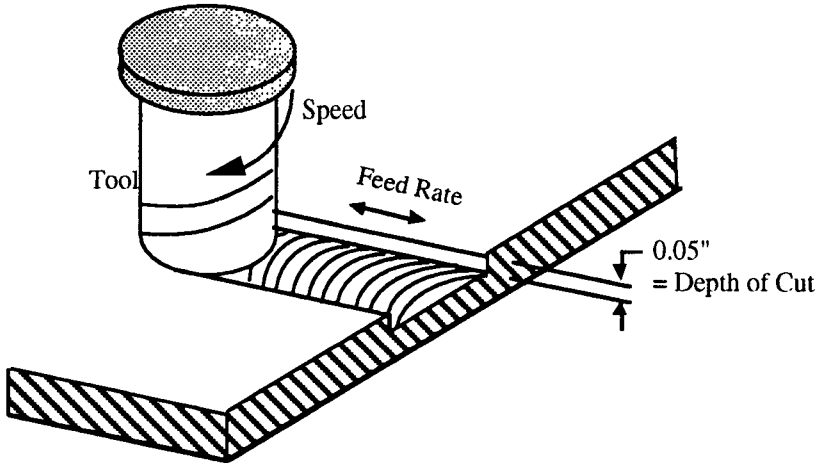

Roughness Parameters	Sample 1	Sample 2	Sample 3	Sample 4	Sample 5
Ra from NIST	0.173	0.211	0.216	0.218	0.269
Fractal Dimension	2.508	2.571	2.585	2.582	2.676

Figure 4.2 Sample preparation

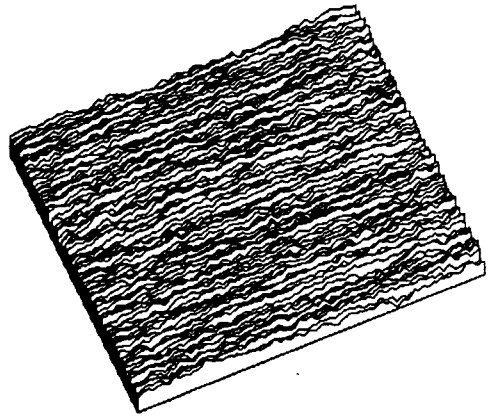

Sample 1 Surface Reconstruction

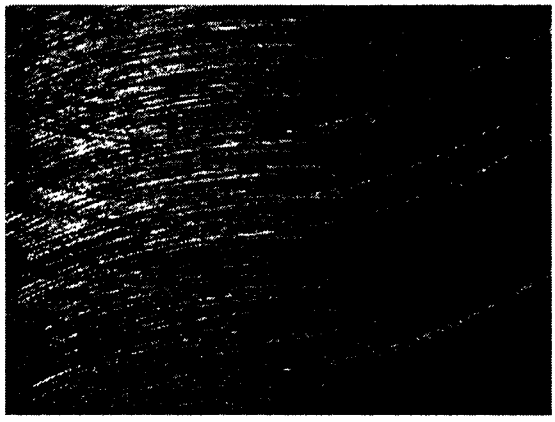

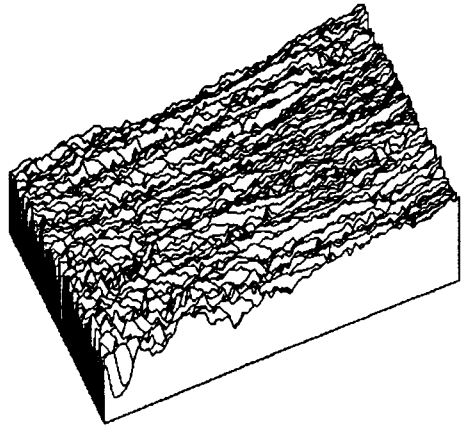

Sample 3 Surface Reconstruction

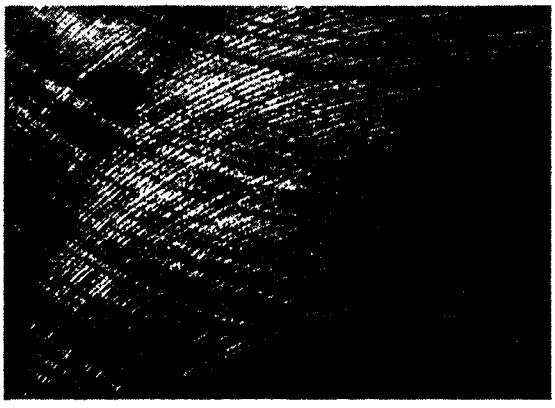

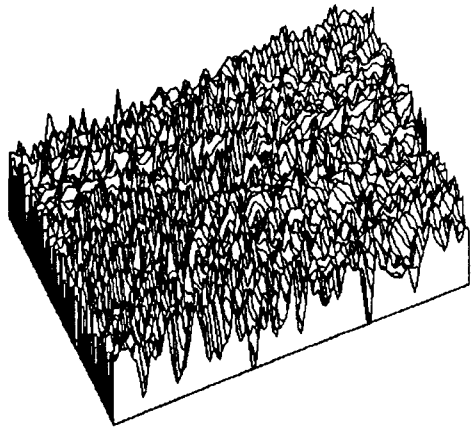

Sample 5 Surface Reconstruction

Figure 4.3 Surface reconstruction from the image of the machined surfaces

From the topographic constructions it is clear that the sample 5, which has the largest Ra value, has the most irregularities, which is much larger than those obtained from sample 1. This observation confirms that the optical inspection method has the capability to distinguish between different patterns of surface roughness. Comparison with the surface profiles obtained from stylus measurement confirms the validity of applying the optical inspection method to surface roughness assessment.

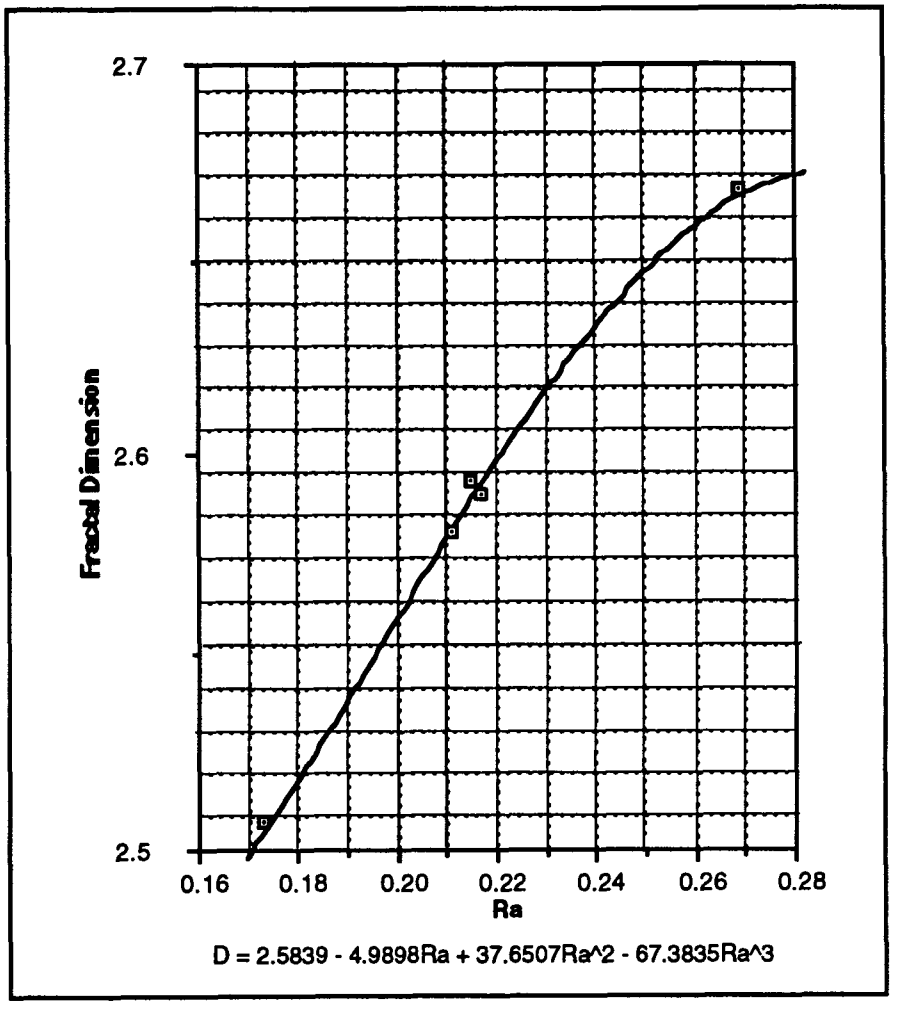

Figure 4.4 Plot between Ra values and fractal dimension

Figure 4.4 a plot between the fractal dimension and Ra values show that the potential of the system in practical applications.

4.3. Sample preparation and measurement apparatus

From the preliminary analysis it was demonstrated that this is a potential alternative to conventional surface roughness assessment methods. For further study, forty aluminum specimens were machined to Ra values ranging from 0.1μm to 1.5μm using a four flute 3/4" diameter end mill. The samples were machined on CNC Matsuura Milling Center. The specimens were machined out of 2" wide blocks using a 0.05" depth of cut under various machining conditions. Various roughness parameters including average roughness (Ra) of the specimens were measured using a calibrated stylus profilometer at the National Institute of Standards and Technology (NIST). The roughness of each sample was determined from the average of five stylus traces over the full width of the milled path, to obtain the true surface roughness as the process used to machine the samples was milling.

4.4. Vision system measurements

4.4.1. Variation of fractal dimension

From previous discussion it has been established that the intensity of light scattered into the overhead camera used in the vision system depends on the roughness of the surface, with the light scattering equation determining the amount of light received by an individual CCD element in the camera. Also that the light received by each element is dependent upon the local roughness and orientation of the surface facets, which comprise

the surface. Thus the image obtained by the vision system is a valid representation of the surface.

For true on line monitoring the fractal dimension calculator must be implemented within the image processing program. The implementation was done using Think Pascal, by modifying the source code of the NIH- Image processing program. The same algorithm used in the UNIX system is implemented but using Pascal language. Now the system is used to measure the fractal dimension directly. From the figure 4.4, it is clear that the fractal dimension is a measure of the surface roughness. This demonstrates that by estimating the fractal dimension, the roughness of the surface can be predicted.

4.4.2. Calibration standard

A 'standard' roughness specimen, which is known to yield a given value of the fractal dimension denoted by D_C, is used to calibrate the system. This specimen is used as the 'standard' when the vision system configuration is disturbed. The vision system is adjusted until the output yields D_C for the standard specimen.

An aluminum roughness specimen of $R_a = 0.45\mu m$ was chosen as the standard calibration surface. Changes are made in the magnification of the camera, light intensity, grazing angle, etc., to obtain the required D_C. Changes made to the light intensity and camera focus were sufficient to reset the system. Light intensity often required slight adjustments due to change in the light input to the CCD camera over a period of several hours, possibly due to fluctuations in the light source power line.

4.4.3. Roughness correlation

After determining the R_a value of the aluminum samples, the optical roughness parameter of each specimen was measured using the vision system, with $\varphi = 10^\circ$ and $\kappa = 45^\circ$. The resulting values of D were plotted against the known roughness values determined at NIST, and a curve fit was performed on the data. The best fit was found to be a third degree polynomial, with a correlation coefficient of $R^2 = 0.85$, The equation of this empirical relationship is given by

D= 2.228 + 0.131Ra + 0.0263Ra^2 - 0.0184Ra^3

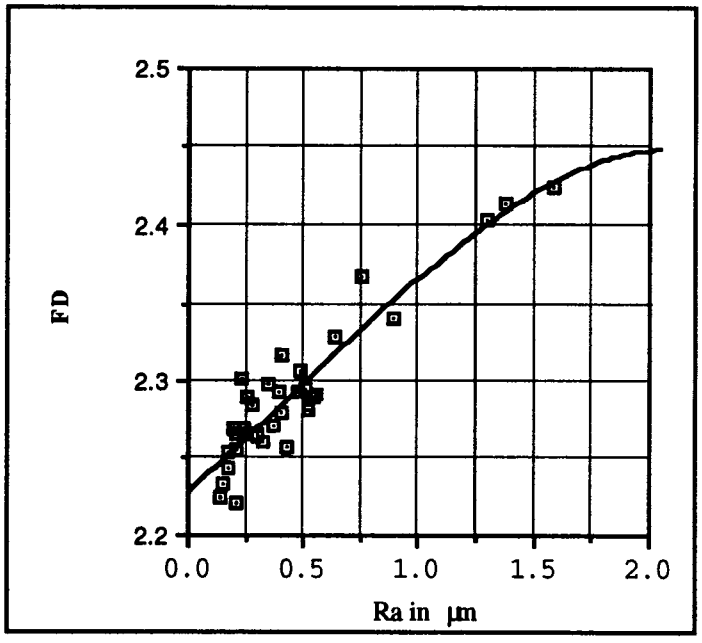

Figure 4.5 Correlation between Ra and fractal dimension (D)

The above calibration curve can be used to determine the roughness of an aluminum workpiece by measuring the fractal dimension, and finding the corresponding R_a.

4.4.4. Sensitivity analysis

During machining, the image of the machined surface may be affected by the environment. Any practical on-line monitoring system must be stable under variation in the environmental conditions. This study is crucial to the implementation of this system as if it was found that the system is too sensitive to these factors, then the system cannot be used to provide accurate surface quality measurements. The four most important factors for system performance were identified and a full 2^4 factorial design was developed and performed on the prototype vision system. The significance of the various factors was then estimated to determine the effects of the variables on the system.

4.4.5. Factors affecting system performance

The system performance was most likely to be affected by the following factors:

1. Ambient lighting
2. Light source brightness
3. Grazing angle
4. Horizontal orientation of light source

The effects of these factors on the system can be hypothesized, based on prior knowledge of the system, fractal geometry and basic light scattering theory. It is known that a two dimensional object has an fractal dimension of 2 whereas a cube would have a

fractal dimension of 3. Therefore the smoother the surface lower will be its fractal dimension. As it becomes rougher and rougher it will fill up the existing space and thereby increasing the fractal dimension. Ambient light increases the brightness level of the pixels and thereby removes the surface detail. This makes the surface look rougher and thus will increase the fractal dimension. The variation in incident angle and the horizontal orientation of the light source is expected to bring out more details or fewer details of the machined surface, due to shadow effect, thus varying the fractal dimension. As the light source becomes more intense the overall image becomes brighter and thus resulting in increase in μ, where μ is the mean value of all the pixels in the image. This again is expected to increase the fractal dimension.

4.4.6. Factorial design

To practically estimate the main effect of these variables, as well as the second and third degree interaction effects on the proposed system a full factorial design with four variables at two levels was done off-line on four different samples with known surface roughness. The levels were chosen to provide moderate variations about the normal levels of the factors. The factorial design is shown in table 4.1.

Factors under Investigation	High Level	Low Level
Horizontal orientation of light source in degrees	55	45
Incident angle of light in degrees	20	10
Light source intensity	100%	80%
Ambient lighting	off	on

Table 4.1 — Factorial design with four variables

A fiber optic cable was mounted on a fixture so that the horizontal orientation and the incident angle of the light can be varied. The level light source intensity was varied by using two settings in the dial. The high level was set at the maximum position and the low level is obtained by reducing the light source brightness to 80% of the maximum setting. Ambient lighting was produced by nine 34W fluorescent bulbs placed between 1.5m to 3m overhead of the experimental arrangement. Sunlight was not allowed to reach the workpiece throughout the experiment. The factorial design used for this experiment is shown in table 4.2. Following the conventional numbering scheme, the four main factors were designated by a number code (1-4) and the two and three factor interactions are designated by the combination of two or three main factor codes. Two factor interaction estimates the variation in the output for variation in two factors simultaneously. For example, two factor interaction between incident angle and light source intensity would be designated as '23' in the table 4.2. The table 4.2 shows the 16 unique combinations of the above effects under which the experiments were performed. The '+' sign indicates high level and '-' sign indicates low level of the factor under consideration.

4.4.7. Significance of effects

The experimental study of any phenomenon is made difficult by the presence of noise sometimes called experimental error. This is also referred as white noise, emphasizing its random nature. The effect of changes in the factors under study, in an experiment, maybe masked due to white noise. The error due to such random and sporadic occurrences is called standard error. In this experiment the standard error is estimated by assuming that the higher order interactions would measure differences arising principally from experimental error. Those effects, which are smaller in magnitude than twice the standard error are assumed to be caused by white noise and thus

do not represent true effects in the measurement process and maybe ignored. From the factorial experiment, the standard error in the measurements was found to be 0.00926.

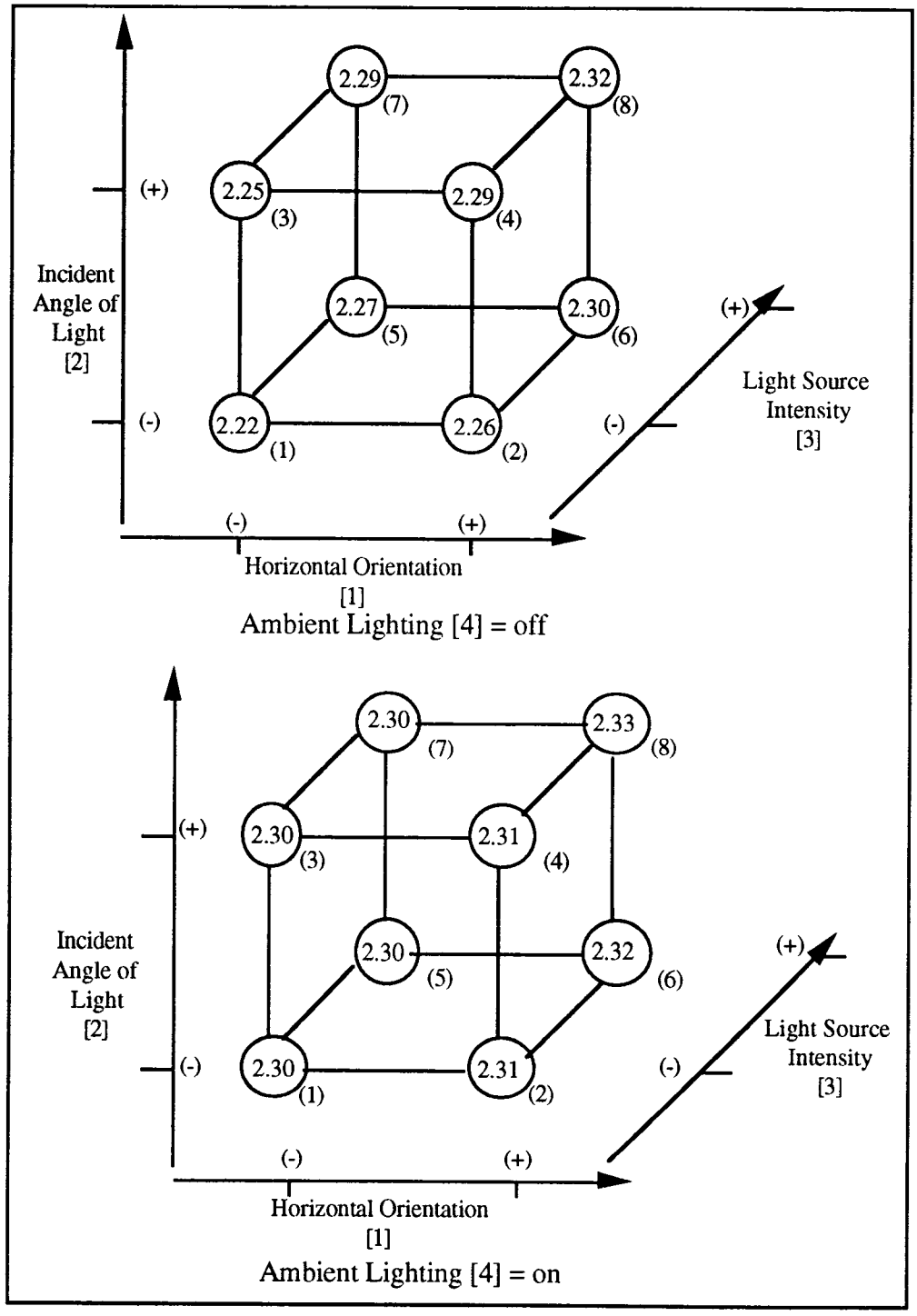

Figure 4.6 Geometric representation of the factorial design of experiments

Runs	Orientation of Light Source	Incident angle of Light	Light Intensity	Ambient Lighting	Calculated Fractal Dimension
1	-	-	-	-	2.2506
2	+	-	-	-	2.3047
3	-	+	-	-	2.2845
4	+	+	-	-	2.3363
5	-	-	+	-	2.2999
6	+	-	+	-	2.3393
7	-	+	+	-	2.3383
8	+	+	+	-	2.377
9	-	-	-	+	2.3493
10	+	-	-	+	2.3611
11	-	+	-	+	2.3589
12	+	+	-	+	2.3681
13	-	-	+	+	2.3596
14	+	-	+	+	2.3781
15	-	+	+	+	2.3671
16	+	+	+	+	2.3892

Table 4.2 — Results from factorial experiment

The significance of the four main effects, six second order effects and two third order effects was estimated. Using the standard error criterion, all second and higher order effects can be neglected as having no significant effect on the system performance. Also the effect of incident angle of the light source can be neglected for small variations in incident angle, with a confidence level of 95%. A mathematical model is generated by the factorial experiment relating the significant factors to the output of the system.

$$D = \text{mean} + k_1X_1 + k_3X_3 + k_4X_4$$

The coefficients from the factorial design are analyzed below in the order of their importance. An important finding is that there is practically no interaction effects between the different factors that affect the sensitivity of the system.

1. Ambient Lighting ($k_4 = 0.05$)

Among all other variables, variation in ambient lighting conditions caused the most variance in the results. Increase in ambient light removes surface detail of the machined surface and thus tends to increase the fractal dimension. Therefore it is very important that the system is calibrated under similar lighting conditions as expected during the actual machining.

2. Source Light Intensity ($k_3 = 0.028$)

The next important variable is the intensity of the light source. Similar to the variation in ambient light, increase in intensity of the light source makes the image more flat and thus the fractal dimension increases. But the light source intensity can be controlled and for small variations in the light source the fractal dimension is not expected to vary by large amount.

3. Horizontal orientation of light source ($k_1 = 0.027$)

Variation in orientation of the light source with respect to the machining direction varies the output of the vision system. This is due to the anisotropic nature of the milled surface. Thus the variation in the surface profile become clearer or hidden, according to the orientation of the light source. Again this requires that the system be properly calibrated. This also requires that the camera orientation system, which makes sure that the camera follows the tool path, be accurate. The solution is to control the position of the camera by a computer controlled stepper motor. The computer gives the commands based on the G-code program.

4. Incident angle of the light source ($k_2 = 0.017$)

Under a confidence level of 95% this effect can be ignored for small variations in the incident angle. This maybe due to the fact that slight variations in the incident angle do not affect the image to produce a measurable variance in output. This result makes the system more reliable if the depth of cut is not constant and the light source need not be adjusted.

4.4.8. Analysis of variance

The above factorial design of experiments were performed on three other samples with different surface roughness resulting in a total of sixty-four data points. Analysis of variance, a widely used technique for decomposing the total variation in a set of data into sources of variation. Each of the variation is considered to be important if it contributes a significant amount of variation to the experimental results. This technique is used to ascertain that the surface roughness causes significant variation in the output of the vision system.

The technique can be summarized as follows. The observed variation in the data is decomposed into sources due to mean, variation between test to test, and variation within a test condition. The variations are squared and summed over all runs and tests. To obtain the pooled variance, the sum of squares is divided by a quantity called 'degrees of freedom'. This quantity is determined based on the test conditions. A null hypothesis is made, that is it is assumed that there is no variation caused by the effect and that the variations observed are purely due to experimental errors. The F value is calculated by dividing the mean square value by the residual error. A significance test is made by observing the corresponding value in an F-distribution available in standard statistic handbooks. If the F_{calc} is more than F_{std} then, the null hypothesis is rejected. Thus the variations due to significant effects and experimental errors can be identified. Generally

the information calculated during an analysis is summarized in the form of a table as shown in table 4.3.

The above analysis of variance test is done on the data observed from the factorial design of experiments. From the values observed in the table clearly the system is very sensitive to changes in the surface roughness as the F-ratio was high for surface roughness variation. It is also evident that small changes in environmental conditions have little effect on the output of the system.

Source of variation	Sum of Squares	Degree of Freedom	Mean Square	Ratio
Grand Average	87.50	1	87.50	
Environmental Conditions	0.0059	3	0.002	12.1
Surface roughness	0.098	3	0.033	198.3
Residuals	0.0015	9	0.0002	
Total		15		

Table 4.3 Results from the F-test

4.5. Additional fractal parameters

As mentioned in the literature survey, many surfaces exist that have the same fractal dimension. In order to make the system more general in application, more parameters can be used to describe the surface. A useful parameter, which describes the surface well is the property of a fractal called lacunarity. In general terms it is a measure of 'gaps' in the surface. It is analogous to the measure of wavelength in curves. Thus measuring the lacunarity of the machined surface would provide a more accurate measure of surface roughness. The methods of measuring lacunarity are available but the process

would require additional processing time. It is trade off between speed and accuracy.

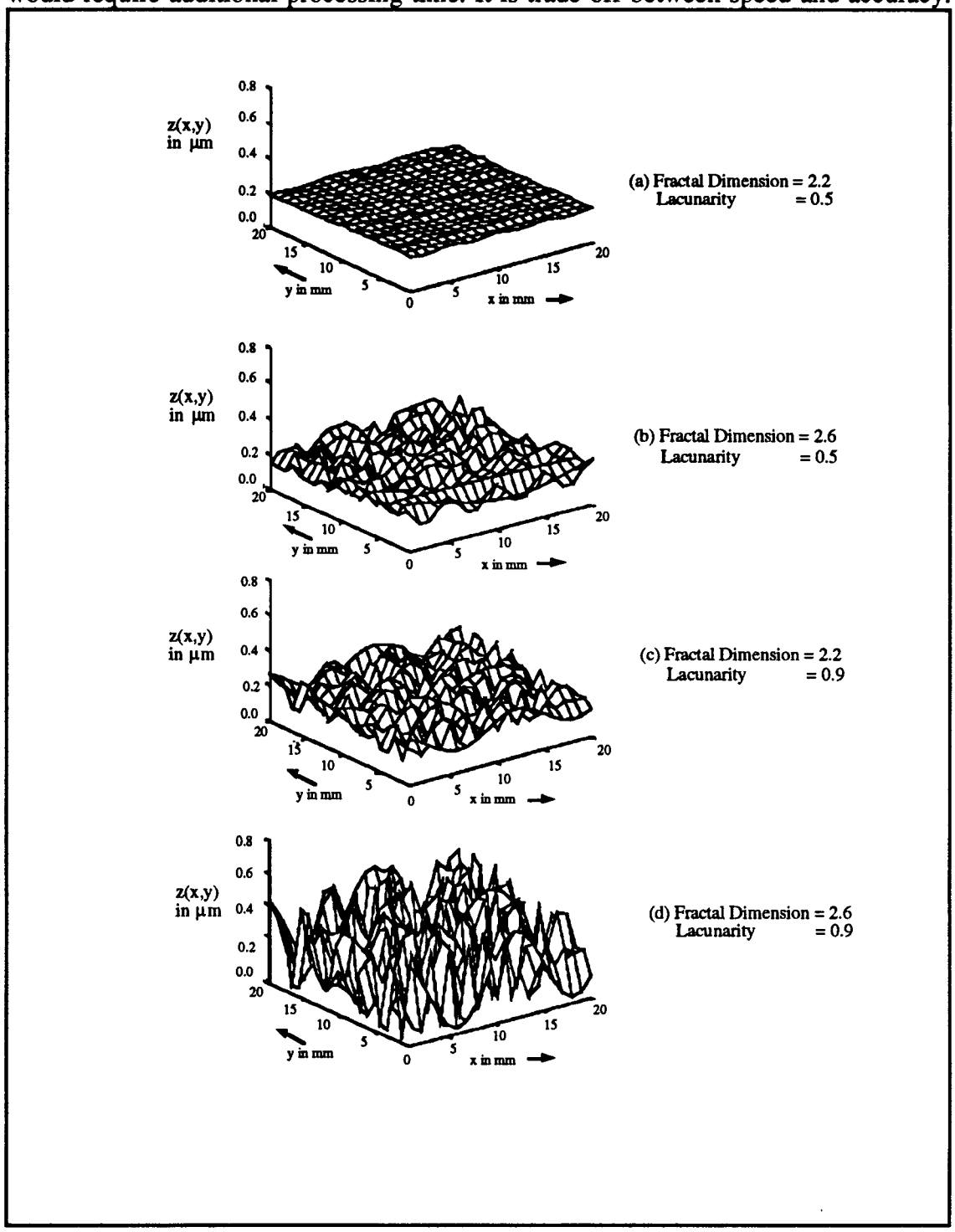

Figure 4.7 Use of additional fractal parameters in surface topography reconstruction

Arrival of faster computers would make such system easily viable. Better visualization can be obtained if lacunarity of the surface is measured along with the fractal dimension of the surface. Reconstuction of surface topography based on fractal parameters is shown in figure 4.7. In the figure, (a) and (c), (b) and (d) have the same fractal dimension but different lacunarity. It can be seen that the roughness is more dependent on the fractal dimension, while the form or waviness is more dependent on lacunarity. Calculation of these two parameters, from the image of machined surface, would produce a better reconstruction of the surface topography. These parameters can then be transmitted to a remote location for further analysis. All conventional parameters that describe surface topography, Ra, Rq, etc., can be determined from the reconstructed surface.

Chapter 5

Testing of vision system on the CNC machine

The algorithm and implementation so far has been done on the prototype system off line. To test the system performance under manufacturing environment a modified vision system to attached to the Matsuura CNC milling center. The results obtained from the tests and the problems associated with performing the analysis on-line is discussed in this chapter.

5.1. Design considerations

There are many of uncontrollable factors that affect the system performance under a machining environment. The vision system must not be totally affected by these factors in order to apply the system to measure surface roughness in order to perform active control of machining operation. Some of the aspects, which makes the vision system measurements more difficult to perform than similar measurements in controlled experimental environment are:

- reflections from machine tool surfaces and other fixtures

- reflections from machine tool surfaces and other fixtures
- coolant
- dynamic movement of camera
- camera / workpiece vibration

For example, reflections from machine tool surfaces may cause interference with the signals from the machined surface. Coolant may obstruct the vision system and result in erroneous readings. Movement of the camera may cause poor resolution of the image. Vibration may also affect the system performance.

A new fixture, the schematic shown in figure, was used to study the effect of above mentioned factors on the system. The main difference between the prototype and the new vision system is the smaller version of the CCD camera (3.5" x 2.5" x 1.5") used instead of the SONY CCD camera. The larger camera cannot be implemented in the CNC machining center due to its larger size.

The apparatus as shown in the photograph and the schematic (figure 5.1 and 5.2), consists of a base ring, which mounts onto the spindle stock of the machine tool, a connecting brace that supports the camera, and a bracket, which mounts the light source onto the camera body. The system configuration can be adjusted to study various effects. Since the apparatus is mounted on the machine spindle stock of the milling machine the camera will move with the machine and as long as the direction of motion is constant the camera will stay focussed on the area being machined. Since the system is only a prototype, a camera with lower resolution is used to save cost and also to show the effectiveness of the system using a low resolution camera.

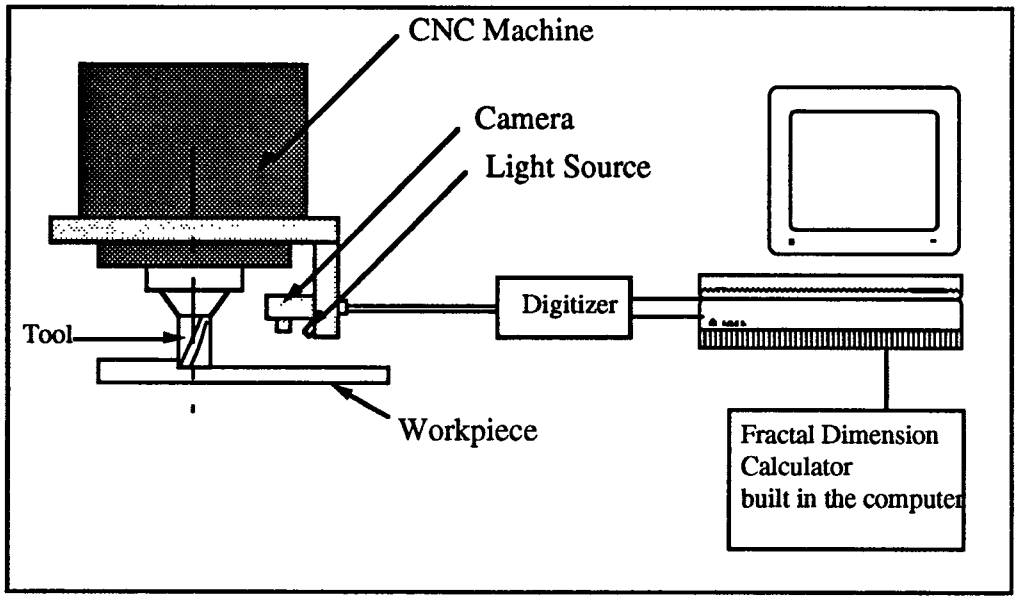

Figure 5.1 Schematic of the implementation of the vision system in the CNC machine

Figure 5.2 Implementation of the vision system in the CNC machine

The vision system can be used with relative ease under dry cutting conditions. However performance under wet cutting conditions presents a challenge since presence of cutting fluid would obscure the vision system. The surface was cleaned carefully during the experiment so that the readings of the vision system would not be affected by the coolant.

As the camera is present very close to the workpiece, the camera is covered with black tape to minimize reflections from the surface of the camera. No modifications were made to the machine tool to simulate the true machining environment, as it would be impractical to modify the machining center to suit the vision system needs.

The feed rates under which the system would reliably operate is unknown. The system should be able to produce reliable results under low feed rate conditions in order to qualify as an on line monitoring system.

5.2. Preparation of calibration samples

In order to calibrate the system for surfaces with varying surface roughness, 40 samples were machined varying the feed rate and spindle speed. The machining conditions were noted so that the experiment could be repeated using new aluminum blocks. Thirty of the forty samples were machined with the coolant, rest where machined dry while blowing air around the tool. The surface roughness of the specimens was then measured in NIST.

The above samples were used to calibrate the vision system and a correlation curve was obtained.

$$D = 2.2868 + 0.5609Ra - 0.366Ra^2 + 0.0966Ra^3$$

The curve, shown in figure 5.3, compares favorably with the calibration curve obtained from the prototype setup, although more scatter is present in the curve obtained from the new setup. The correlation coefficient is 0.73 while it was 0.85 on the prototype system. This can be attributed to the lower resolution of the camera, the effects of variation in ambient lighting and surface reflections.

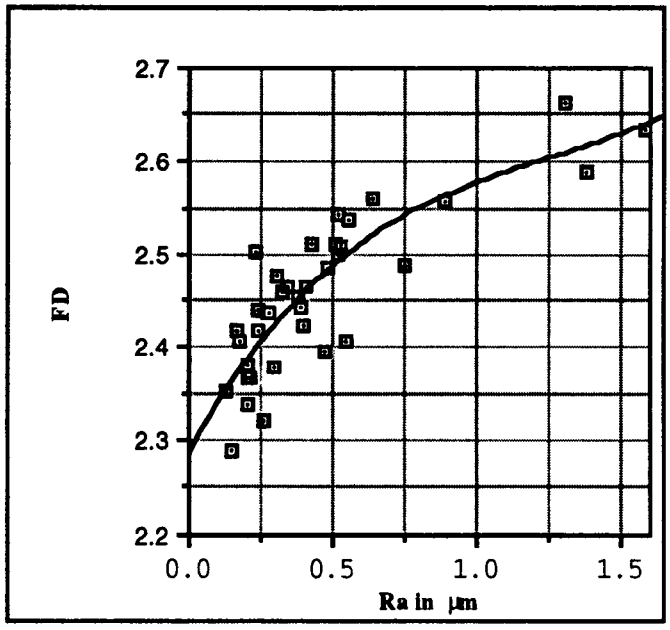

Figure 5.3 Correlation curve between D and Ra

5.3. System Performance during machining operation

Under the same conditions as existing for the calibration process, the machining was done under the same conditions to study the performance of the system under actual machining operation. Extreme care was taken to remove the coolant from the camera and its region of interest. The roughness of the image was estimated by using the calibration curve generated by measuring the system output from the previously machined samples. The error between the estimated and the true values was calculated as shown in the form in figure 5.4.

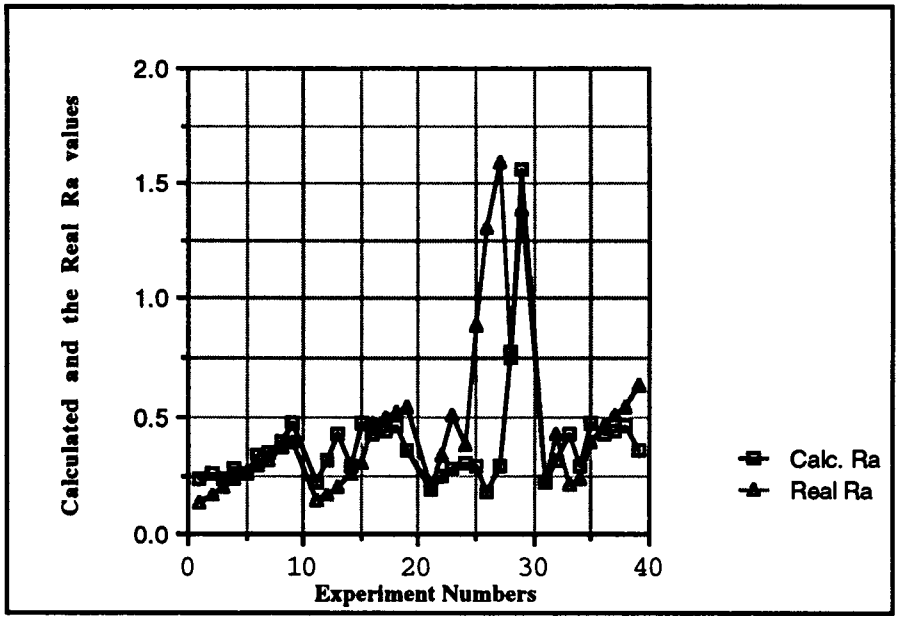

Figure 5.4 Comparison of the calculated and the real Ra values

In general the error range is around 0.1-0.2μm, which is satisfactory considering the adverse conditions under which the system is operated. The average error is 0.17μm with a standard deviation of 0.28μm. The minimum error is 0.0005μm and the maximum error is 1.3μm. The ease under which these values were obtained and the fact that these measurements were made under actual machining makes the system a practical on-line monitoring system. The effectiveness of the system under actual machining conditions is thus demonstrated.

5.4. System performance under motion

In all the above experiments the feed rate was varied from 1.0 in/min. to 5.0in/min. In the industry however much higher feedrates would be used and the performance of the system under such conditions is studied in this section. The testing was done by mounting the apparatus on the CNC machine and programming the machine such that a sample of known surface roughness is measured under different feed rates.

Three measurements were taken over the area under for each feed rate. The variations in the system output with respect to the true values were then examined to evaluate the system performance. The true value was obtained by obtaining the fractal dimension when the sample was stationary.

Feed Rate	Measured Fractal Dimension	True fractal dimension	Error
0.0	2.4325	2.4325	0
0.8	2.4321	2.4325	0.0004
1.2	2.4322	2.4325	0.0003
4.0	2.4313	2.4325	0.0012
7.0	2.4302	2.4325	0.0023
10.0	2.4104	2.4325	0.0221
15.7	2.3927	2.4325	0.0398
19.7	2.3665	2.4325	0.066
23.6	2.3178	2.4325	0.1147
47.3	2.2856	2.4325	0.1469
59.0	2.2598	2.4325	0.1727
78.7	2.2436	2.4325	0.1889
118.0	2.2260	2.4325	0.2065
		Standard Error	0.0005

Table 5.1 Effect of feedrate on the vision system

The output of the system is tabulated in the table. The experimental or standard error was measured by calculating the standard deviation that was present in ten measurements of the stationary sample. Any reading whose difference from the mean is greater than the twice the experimental error is taken to be a significant reading. The significant readings are also shown in the table. From the table, it is clear that changes in the reading with respect to the feedrate cannot be accounted for by purely natural variations in the measurements. Therefore the feedrate has a significant effect on the system performance.

greater than the twice the experimental error is taken to be a significant reading. The significant readings are also shown in the table. From the table, it is clear that changes in the reading with respect to the feedrate cannot be accounted for by purely natural variations in the measurements. Therefore the feedrate has a significant effect on the system performance.

The figure 5.5 shows four images captured by the vision system for a range of feed rates, from stationary to 118in/min. As the feed rate increases, the image quality deteriorates. The image until the feed rate of 7.0 in/min. is virtually unchanged and the individual machining marks can be identified. In the third image, obtained for a feed rate of 23.0 in/min. the machining marks are no longer clear and the picture is blurred. For feed rate of 118 in/min., a severely blurred and picture exhibiting 'double image' effect is obtained. While a feed rate of 118 in/min. is rarely used in manufacturing, the image illustrates the problems associated with measuring the surface roughness of a moving workpiece.

This behavior can be explained in part by the video system used to capture the image. The standard NTSC (National Television Standards Committee) system is used to monitor the machined surface. NTSC video is composed of two sets of raster groups, where each group is offset from the other by one scan line. Thus, the CCD image is captured by sampling every other scan line of the image, from top to bottom, and then repeating the same scanning process but with an offset of one scan line. This procedure of scanning results in an image in which the two adjacent scan lines are not scanned at the adjacent moments of time, but rather separated by half of the time required to scan the entire image. Thus with the frame grabber operating at 30 frames per second, two adjacent scan lines are separated by 1/60 s gap. This effect is a feature called interlace video, which is used by NTSC to reduce eye strain.

Feed Rate =0.0 Fractal Dimension = 2.4325

Feed Rate =7.0 Fractal Dimension = 2.4302

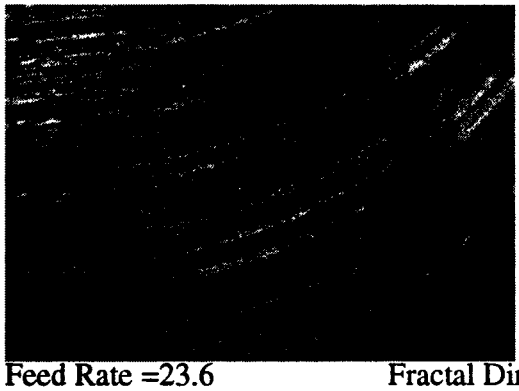

Feed Rate =23.6 Fractal Dimension = 2.3178

Feed Rate =118.0 Fractal Dimension = 2.2260

Figure 5.5 The effect of feedrate on the output of the vision system

The effect of the interlacing is that a double image is obtained by the vision system when the workpiece is moving at a faster rate. This effect can be explained by examining the relationship between the feedrate and the image obtained. Consider a workpiece examined by the vision system moving at a feedrate of 1in/min. Due to a combination of the time lag between capturing adjacent scan lines and the motion of the workpiece, any two adjacent scan lines will show sections of the surface, which are separated by a distance of

$$\left[\frac{1}{2}\times\frac{1}{30}\text{sec}\right]\left[1\frac{\text{in}}{\text{min}}\right]\left[\frac{1\text{min}}{60\text{sec}}\right]=0.00028\text{in}$$

Thus in the case of a workpiece moving at 118in/min., the distance between adjacent scan lines will be 118 x 0.00028 in = 0.0333in. The actual separation distance is measured from the image and is found to be 0.031in, which agrees with the theoretical separation distance of 0.0333in, suggesting that interlacing process is the cause of image blurring occurring at high feed rates. Therefore the difficulty in obtaining clear images from the system is a result of the intrinsic property of the video acquisition system and not a defect in the vision system.

Chapter 6

Conclusions and recommendations

6.1. Conclusions

A prototype system is developed to perform surface roughness measurements using an area based fractal approach, which makes it especially suitable for on-line process monitoring. The theoretical basis for this approach using fractal geometry and optical methods is presented. The validity of modeling the surface as a fractal is also shown. Using electromagnetic wave scattering theory the relation between the observed image and the true surface topography is obtained. The results show that the fractal dimension of the image can be used to estimate the surface roughness.

In order to determine whether fractal geometry can be used to model machined surfaces, a fast algorithm is developed on unix mainframe to obtain the fractal dimension of the images. This algorithm is used to analyze the images of surfaces with varying surface roughness off-line. The results show a good correlation between the surface

roughness and fractal dimension of the image. The algorithm is then incorporated in the image processing software so that the analysis can be made on-line. A functional calibration curve, which relates the fractal dimension of the surface to the surface roughness was constructed in this thesis. The close correlation between the fractal dimension and surface roughness shows that the developed vision system provides a cost effective method for on-line monitoring. A sensitivity analysis is made using factorial design of experiments to demonstrate the effect of the environment on the system. One of the significant findings in this study is that the calculated fractal dimension is sensitive enough to detect the variation in the surface finish even under different ambient conditions. The challenge in implementing this system is that the calibration process should be done under the same conditions that exist in the machining environment.

The system is implemented on the CNC machine using a miniature CCD camera to demonstrate its viability in an industrial environment. Experiments were conducted under both dry and wet milling conditions. The results show that the system performs adequately even under the extreme conditions of machining environment. Thus the potential for integrating such a device into an active machining control system is demonstrated.

While the system performed well under feed rates of 10in/min., higher feed rates impair the system output. The cause of this problem is identified as an attribute of the video acquisition system. Use of advanced hardware can eliminate or reduce the problem. One way is to implement a non interlacing video camera system. Non interlacing cameras are available but are expensive. Also frame grabbers with higher frame rates can be used. Another method is to compensate for the shift in the double image using image manipulation as the feed rate can be obtained from the CNC program. Such a

manipulation would require a faster processor as image manipulation is computationally intensive process.

The potential of this system as a practical surface roughness measurement system is thus demonstrated. This system can be used as a tool to maintain surface quality throughout the machining process.

6.2. Future work

At present the system is not interfaced with the G-code program that will perform the machining on the CNC machine. This presents some problems which are discussed here. In order to realize the system truly the system must be able to draw motion parameters from the G-code program.

The camera fixture is fixed in orientation with respect to the feed direction. In order to applied in a practical environment a rotary head system must be used such that the camera may be able to follow the tool motion in all directions. A design of a rotary structure was made and partially built for this study. The system should use the G-code program to determine when the cutting is done and the direction to follow.

The image processing software must be able discern between the machined surface and the surfaces not affected by machining. This involves knowledge of the tool diameter, depth of cut and a control system, which would move the camera up or down depending on the above mentioned parameters. Such a control is possible by controlling the software based on the G-code program and feeding the tool geometry to the vision system.

Use of fiber optic cameras that are commercially available would make the system more practically viable. Adjustments to the camera by the control system can be made much easily as fiber optic cameras are very light in weight. Study should be made on incorporating fiber cameras in the vision system.

Presence of coolant during machining was dealt in this study by blowing away the coolant during the machining process. It is recognized that the above is not always possible. Experiments should be done finding a wavelength of light that can pass through the coolant with slight refraction. Such a system would require a special camera that would be sensitive to the wavelength under which the effect of coolant is not observable. Also the wavelength used must be safe to human operators. A calibration curve made after blowing the coolant of a standard roughness workpiece would perform adequately with a proper coolant blowing system.

Additional fractal parameters like lacunarity can be used to describe the surface more accurately. Fast algorithms should be developed to measure the lacunarity and other fractal parameters. Such a system would have great potential in wireless communication of surface topographical information with minimal number of parameters.

Appendix A

Some of the results obtained from various analyses mentioned in the thesis, are listed here.

Table 1: Sensitivity analysis

	O.L	I.A	L.I	A.L	F.D
1	-1	-1	-1	-1	2.25056
2	1	-1	-1	-1	2.30469
3	-1	1	-1	-1	2.28453
4	1	1	-1	-1	2.3363
5	-1	-1	1	-1	2.29993
6	1	-1	1	-1	2.33926
7	-1	1	1	-1	2.33832
8	1	1	1	-1	2.37697
9	-1	-1	-1	1	2.34932
10	1	-1	-1	1	2.36113
11	-1	1	-1	1	2.3589
12	1	1	-1	1	2.36805
13	-1	-1	1	1	2.35955
14	1	-1	1	1	2.37809
15	-1	1	1	1	2.36708
16	1	1	1	1	2.38923

where

O.L = Orientation of Light Source

I.A = Incident Angle of the Light on the workpiece

L.I = Light Intensity

A.L = Ambient Light

Table 3: Variation of calculated fractal dimension during actual machining process along with the mean Ra values calculated by the profilometer at NIST

S800		S900	
Ra value from NIST	Calculated Fractal Dimension	Ra value from NIST	Calculated Fractal Dimension
0.228	2.22624924	0.205	2.21228252
	2.24584476		2.20873596
	2.58332173		2.2048546
	2.2624631		2.20903541
	2.29861034		2.21814644
	2.27843318		2.27573898
	2.21307933		2.2179215
Mean	2.30114309	Mean	2.22095934
0.429	2.22002698	0.3425	2.25564183
	2.24794566		2.29107621
	2.28035519		2.32898327
	2.27142582		2.31630471
	2.22637206		2.24775825
	2.24198688		2.33123051
	2.30335744		2.31394234
Mean	2.25592429	Mean	2.29784816
0.213	2.24702109	0.515	2.29914984
	2.22373269		2.28824709
	2.25494069		2.23020115
	2.2412764		2.33946829
	2.27066785		2.28265689
	2.30048722		2.27366979
	2.24076277		2.24472856
Mean	2.25412696	Mean	2.27973166
0.2445	2.28084204	0.3895	2.29950435
	2.22446057		2.27367373
	2.31646244		2.30729589
	2.23898379		2.34362279
	2.27057859		2.31453075
	2.28437632		2.28094755
	2.26846824		2.22282232
Mean	2.26916743	Mean	2.29177105

Table 3: Variation of calculated fractal dimension during actual machining continued

0.402	2.24825351	0.89	2.37374267
	2.27919915		2.36934712
	2.27113898		2.27607019
	2.28098283		2.38934821
	2.31487603		2.3446648
	2.23518332		2.3221824
	2.32509026		2.31064364
Mean	2.2792463	Mean	2.340857
0.469	2.2982531	1.3	2.44516009
	2.2832053		2.51135437
	2.3192768		2.24257089
	2.31309384		2.58155261
	2.23095718		2.28891186
	2.33353622		2.50751287
	2.27081927		2.25176127
Mean	2.29273453	Mean	2.40411771
0.5145	2.26691916	1.585	2.34092685
	2.29941756		2.57691549
	2.37703286		2.55077539
	2.27212916		2.34235946
	2.2353018		2.30555164
	2.26078479		2.49049476
	2.27934665		2.36733378
Mean	2.28441885	Mean	2.4249082
0.5515	2.31802846	0.75	2.40698921
	2.22011714		2.32787536
	2.27378089		2.30415738
	2.26866385		2.35575871
	2.34595617		2.32167845
	2.31466169		2.4493191
	2.28905484		2.4084072
Mean	2.29003758	Mean	2.36774077
0.64	2.29492578	1.38	2.59714854
	2.38501331		2.4028671
	2.21809591		2.41415166
	2.31999399		2.33741747
	2.35172603		2.24989257
	2.36512747		2.41815856
	2.36115358		2.47867065
Mean	2.32800515	Mean	2.41404379

Table 3: Variation of calculated fractal dimension during actual machining continued

S1000		S1100	
0.1485	2.20200936	0.133	2.19965899
	2.20228166		2.19892538
	2.2010732		2.19967461
	2.2002891		2.19917919
	2.25046173		2.28691078
	2.2993211		2.25998487
	2.27122832		2.22141809
Mean	2.23238064	Mean	2.22367884
0.168	2.2771041	0.174	2.25832465
	2.2268471		2.2818108
	2.2133823		2.25344273
	2.28439542		2.21073761
	2.20849255		2.25217113
	2.23785481		2.21746971
	2.25087669		2.30013973
Mean	2.24270756	Mean	2.25344234
0.202	2.28812815	0.2045	2.29475548
	2.26362333		2.25566943
	2.27452726		2.31261767
	2.24277608		2.27138557
	2.28441949		2.26157305
	2.28727072		2.22335385
	2.23847582		2.23146809
Mean	2.26846012	Mean	2.2644033
0.2585	2.32044035	0.243	2.2836558
	2.29799539		2.25927524
	2.29431411		2.22609355
	2.27384166		2.27466962
	2.28919411		2.26351844
	2.24458521		2.2419895
	2.30663735		2.30288215
Mean	2.2895726	Mean	2.26458347
0.305	2.25667308	0.277	2.3073424
	2.27195042		2.31705904
	2.2410744		2.33222586
	2.21617969		2.22611876
	2.29765227		2.28548335
	2.28807431		2.28912397
	2.29031377		2.22661716
Mean	2.26598828	Mean	2.28342436

Table 3: Variation of calculated fractal dimension during actual machining continued

0.4825	2.26304349	0.2965	2.23154847
	2.32502659		2.2207423
	2.29142623		2.29800808
	2.32286596		2.25896905
	2.33007335		2.29961129
	2.32602124		2.26892788
	2.29074858		2.26442366
Mean	2.30702935	Mean	2.26317582
0.5045	2.30900703	0.325	2.26084956
	2.2736715		2.26605142
	2.37682787		2.21788041
	2.28384226		2.28742209
	2.25916479		2.29285794
	2.2651359		2.27469827
	2.28704396		2.22036765
Mean	2.29352761	Mean	2.26001819
0.5295	2.32427753	0.375	2.25130248
	2.31242228		2.24915981
	2.28539355		2.28676842
	2.30995705		2.30304476
	2.28748299		2.25525447
	2.25054742		2.29471154
	2.25259377		2.25342022
Mean	2.28895351	Mean	2.2705231
0.5435	2.35348022	0.405	2.2781339
	2.2832255		2.36604652
	2.29516978		2.3367007
	2.23657085		2.30945221
	2.30535174		2.3106872
	2.26687493		2.35382046
	2.2890093		2.25842529
Mean	2.28995462	Mean	2.3161809

Table 4: Values obtained from NIST

FeedRate	Ra	Rq	Ry	Rtm	Rv	Rp	Rpm
1	0.223	0.296	2.41	1.86	1.48	1.15	0.93
	0.233	0.331	2.78	2.2	1.27	1.54	1.18
	0.228	0.3135	2.595	2.03	1.375	1.345	1.055
1.2	0.305	0.41	2.74	2.22	0.95	2	1.38
	0.553	0.704	4	3.18	1.9	2.73	1.83
	0.429	0.557	3.37	2.7	1.425	2.365	1.605
1.4	0.241	0.306	2.35	1.72	0.82	1.53	1.06
	0.185	0.233	1.38	1.25	0.64	0.77	0.7
	0.213	0.2695	1.865	1.485	0.73	1.15	0.88
1.6	0.284	0.364	2.41	2.17	0.94	1.47	1.31
	0.205	0.254	1.44	1.25	0.78	0.65	0.56
	0.2445	0.309	1.925	1.71	0.86	1.06	0.935
1.8	0.499	0.592	2.91	2.51	1.121	1.69	1.35
	0.305	0.385	2.56	1.92	0.93	1.69	1.1
	0.402	0.4885	2.735	2.215	1.0255	1.69	1.225
2	0.528	0.617	2.88	2.63	1.27	1.71	1.43
	0.41	0.503	2.15	2.06	1.09	1.19	1.1
	0.469	0.56	2.515	2.345	1.18	1.45	1.265
2.2	0.588	0.701	4.74	3.28	1.9	2.85	1.85
	0.441	0.543	2.59	5.38	1.18	1.5	1.31
	0.5145	0.622	3.665	4.33	1.54	2.175	1.58
2.4	0.618	0.705	3.09	2.8	1.72	1.4	1.27
	0.485	0.59	3.09	2.62	1.62	1.74	1.42
	0.5515	0.6475	3.09	2.71	1.67	1.57	1.345
2.6	0.693	0.819	4.24	3.52	2.2	2.72	1.58
	0.587	0.733	4.14	3.45	1.93	2.25	1.81
	0.64	0.776	4.19	3.485	2.065	2.485	1.695

Appendix B

Hardware Specifications

(1) Camera used in the algorithm testing system

Manufacturer	Sony
Model	SSC-M350 monochrome CCD video camera
Specifications	1/2" Inter-line transfer type monochrome CCD
Resolution	510 (horizontal) x 492 (vertical)
Automatic gain control:	switched off
Video out:	NTSC

(2) Miniature camera mounted on the CNC machine

Manufacturer	Supercircuits
Model	PC-3 microvideo camera
Specifications	1/3" MOS monochrome CCD
Resolution	324 (horizontal) x 246 (vertical)
Video out:	NTSC

(3) Frame Grabber

Manufacturere	Data Translations
Model	QuickCapture frame grabber board
Specifications	NTSC, monochrome interlaced

Resolution	640 (horizontal) x 480 (vertical)
Frame grab speed:	1/30 second
Aspect ratio:	1:1 (square pixels)

References

[BDV88] Barnsley, R.L. Devaney, R.F. Voss, The Science of Fractal Images, Springer-Verlag, NewYork, 1988.

[BS63] Beckman P, Spizzichino A., "The Scattering of Electromagnetic Waves From Rough Surfaces," Oxford:Pergamon, 1963.

[BD81] Bennett J. M., Dancey J. H., Stylus Profiling Instruments for Measuring Statistical Properties of Smooth Optical Surfaces, Appl. Opt. 20, p 1785, 1981

[BM89] Bennett J. M., Mattson L., Introduction to Surface Roughness Scattering, Optical Society of America, 1989

[BGT85] Brodman R., Gerstorfer O., Thurn G., Optical Roughness Measuring Instrurnent for Fine Machined Surfaces, Opt. Eng. 24, 408, 1985

[CHR79] Church E. L., The Measurement of Surface Texture and Topography by Differential Light Scattering, Wear, 57, 93-105, 1979.

[DM85] Detrio J. A., Miner S. M., "Standardized Total Integrated Scatter Measurements of Optical Surfaces," Opt. Eng. 24, 419,1985.

[DEV93] DeVoe, 1993," Optical Area based Surface Quality Assessment for In-Process Measurement", Masters Thesis, University of Maryland, College Park

[DF86] Dornfeld D. A., Fei R. Y., In Process Surface Finish Characterization, ASME. Prod. Eng., Division PED 20,191-204, 1986.

[GV86] Gilsinn, T. Vorburger et al., "Optical Roughness Measurements of Industrial Surfaces", Optical Techniques for Industrial Inspection, Vol. 665, 1986.

[LT89] Larry S. Liebovitch and Tibor Toth, "A Fast Algorithm to determine Fractal Dimension by Box Counting", Physics Letters A, volume 141, n 8.9, 1989.

[LNG90] Ling, "Fractals, engineering surfaces and tribology",Wear,1364, 1990.

[LHN89] Luk F., Huynh V., North W., Measurement of Surface Roughness by a Machine Vision System, Journal of Physics E: Scientific Instruments 22, 977-80,1989.

[MB90] Majumdar A. and Bhushan B., "Role of Fractal Geometry in Roughness Characterization and Contact Mechanics of Surfaces", Journal of Tribology, Vol. 112, 1990.

[MT90] Majumdar A. and C.L.Tien, "Fractal characterization and simulation of rough surfaces", Wear, Vol. 136, 1990.

[MB82] Mandelbrot Benoit B. , Fractal Geometry of Nature, W.H. Freeman, New York, 1982.

[MB85] Mandelbrot, B. B.,"Self-affine fractals and the fractal dimension", Physics Scripta , v 32, 1985.

[SM66] Saya T., Moritada K., On the Forming of Surface Roughness in Finished Processing, Bull. the Japan Soc. of Prec. Eng. 1, 4, 287-293, 1966

[SRS82] Sayles R. S., "Rough Surfaces," T. R. Thoma, Ed., Longman, London, 1982

[SA86] Stephen F. Attali, F.S. Cohen, "Surfae inspection based on stochastic modeling", Optical Techniques for Industrial Inspection, Vol. 665, 46-52, 1986

[TTR82] Thomas T. R., Ed., "Rough Surfaces," Longman, London, p 189,1982

[TV57] Twersky V., On the Scattering and Reflection of Electromagnetic Waves by Rough Surfaces, Trans. I.R.E. AP-5, 81-90, 1957.

[VO92] Vandenberg and C.F. Osborne, "Digital image processing techniques, fractal dimensionality and scale-space applied to surface roughness", Wear, Vol. 159, 1992.

[VR90] Vorburger T., Raja J., "Surface Finish Metrology," NISTIR-4088, U. S. Dept. of Commerce, 1990.

[VRF85] Voss, R.F., "Random Fractal Forgeries,", in Fundamental Algorithms for Computer Graphics, ed. R.A. Earnshaw, 1985.

[WM93] Wielinga T, Mellissant J., "New optical devices for surface roughness measurements ", Journal of magnetism and magnetic materials, Vol. 120, 1993

[ZVM89] Zimmerman J. H., Vorburger T. V., Moncarz H. T., "Automated Optical Roughness Inspection," Optical Testing and Metrology II, Proc. SPIE 954, 252, 1989